J. Plasma Physics (1997), *vol.* 58, *part* 3, *pp.* 521–552. Printed in the United Kingdom
© 1997 Cambridge University Press

Shock waves and rarefaction waves in magnetohydrodynamics. Part 2. The MHD system

R. S. MYONG† and P. L. ROE

W. M. Keck Foundation Laboratory for Computational Fluid Dynamics, Department of Aerospace Engineering, University of Michigan, Ann Arbor, Michigan 48109, USA

(Received 4 February 1997)

In Part 1 of this study, a model set exactly preserving the MHD hyperbolic singularities was considered. By developing the viscosity admissibility condition, it was shown that the intermediate shocks are necessary to ensure that the planar Riemann problem is well-posed. Here in Part 2, the MHD Rankine–Hugoniot condition and rarefaction-wave relations are presented in phase space, which allows construction of analytical solutions of the planar MHD Riemann problem. In this process, a viscosity admissibility condition is proposed to determine physically admissible shocks. A complete account of MHD Hugoniot loci is given, leading to a classification of several subproblems in which the solution patterns are qualitatively same. Finally, it is shown that the planar MHD Riemann problem is well-posed using intermediate shocks that have been considered non-evolutionary.

1. Introduction

In the theory of ideal magnetohydrodynamics (MHD) a variety of rather complex wave phenomena are possible. This is related to the fact that magnetoacoustic waves are non-convex, meaning that an increase in density with respect to time sometimes causes a convergence of characteristics and sometimes a divergence. Because of this, discontinuities that satisfy the Rankine–Hugoniot jump conditions cannot always be associated with a particular characteristic family out of whose simple waves the discontinuity can be supposed to have evolved. The question therefore arises to which of these discontinuities are admissible for the construction of weak solutions to the MHD equations.

A substantial literature exists on this problem, leading to the so-called *evolutionary condition* (Akhiezer *et al.* 1959, 1975; Jeffrey and Taniuti 1964; Kantrowitz and Petschek 1966; Blokhin 1994), from which it can be concluded that no discontinuity (excepting a *rotational discontinuity*) is able to reverse the sign of the transverse magnetic field. It is known, however, that if only evolutionary shocks are employed, not all Riemann problem have solutions (Jeffrey and Taniuti 1964, pp. 256–269;

† Present address: NASA Goddard Space Flight Center, Mail Stop 930, Greenbelt, Maryland 20771, USA

https://doi.org/10.1017/S0022377897005941 Published online by Cambridge University Press

Polovin and Demutskii 1990, pp. 151–157). The failure of the evolutionary condition has become apparent since several researchers investigated the MHD Riemann problem numerically. In a series of numerical experiments, Wu (1987, 1990, 1995) identified intermediate shocks embedded in compound waves from the numerical solutions to the full MHD equations. However, for lack of a rigorous analytical theory for these intermediate shocks, this finding has not drawn much attention. Therefore it was often considered true that the MHD planar Riemann problem possesses no known analytical solution.

In this paper, we present the MHD Rankine–Hugoniot condition and rarefaction wave relations in a useful form. In this process, a mathematical theory that was developed from the model (Myong 1996; Myong and Roe 1997*b*) is applied to the MHD system. As a result, the weak solutions of the planar MHD Riemann problem are constructed. Strictly speaking, we consider only half of the Riemann problem. That is, instead of specifying left and right states $\mathbf{u}_L$ and $\mathbf{u}_R$, we specify one of $\mathbf{u}_L$ and $\mathbf{u}_R$, together with a state $\mathbf{u}_M$ on one side of the contact discontinuity, so that the two given states are separated only by right-running (or left-running) waves. For this restricted problem, our result is rigorous, because we can exhaustively treat all the cases. We do claim, however, that any complete Riemann problem can be reduced in a unique way to two half-Riemann problems, and we give arguments to make this claim plausible. If the claim is true then of course it follows that the same set of discontinuities is necessary and sufficient for the full problem. Note that Alfvén waves play no part in our planar solution by definition, since an Alfvén wave must rotate the transverse field out of its initial plane. However, this does not mean that field rotation by a rotational discontinuity is prohibited from the formulation. In fact, field rotation is possible even in planar problems by a transverse discontinuity with a jump of an angle of 180°, which corresponds to a special case of undercompressive shocks. Therefore the question is which of intermediate shock and rotational discontinuity can change the sign of the transverse field vector. In this study, we show that change of sign in the transverse field has to be supplied by the intermediate shocks.

This paper is organized as follows. In Sec. 2, we consider the planar Riemann problem and develop the basic properties of MHD shocks and simple waves. Much of this material is classical, but we also present a rather simple and useful form of the MHD Hugoniot, which we believe to be new. We relate these properties to recent mathematical theories of shock selection. In addition, we give a complete account of all possible Hugoniot loci. This leads also to a listing of all possible mechanisms by which the transverse field of a given state may be reversed. Then we develop a unique solution to the planar Riemann problem. We follow very closely the presentation in Schaeffer and Shearer (1987*a*) and Isaacson *et al.* (1988) for their model problem. We aim at giving sufficient detail to make the account self-contained, but the references should be consulted for the finer points. In Sec. 3, we consider the non-planar problem and derive the relationship between the model and the MHD system. In Appendix A, we study the MHD dynamical system and develop a viscosity admissibility condition. In Appendix B, several critical curves for the existence of certain shocks are identified. Finally, in Appendix C, a mathematical proof is given of the exact relevance of the model and the MHD system.

From a practical standpoint, it may be objected that the planar MHD problem is an artificial one, never precisely found in nature. Nevertheless, situations that are nearly planar are encountered, and although any abnormal waves that are

https://doi.org/10.1017/S0022377897005941 Published online by Cambridge University Press

produced may be expected to decay under non-coplanar perturbations (Ugai and Shimizu 1994), there is evidence that this decay may be rather slow. Therefore we believe that the overcompressive and compound waves studied here must be accounted for in any comprehensive numerical simulation of MHD.

2. Planar MHD

2.1. MHD Rankine–Hugoniot relations

From the ideal MHD equations in the Lagrangian description, the MHD shock relations are expressed as follows (Jeffrey and Taniuti 1964):

$$m[\tau] - [u] = 0, \tag{2.1}$$

$$m[u] + [p] + \bar{B}_\perp[B_\perp] = 0, \tag{2.2}$$

$$m[v] - B_x[B_\perp] = 0, \tag{2.3}$$

$$m\bar{\tau}[B_\perp] + \bar{B}_\perp[u] - B_x[v] = 0, \tag{2.4}$$

$$m[e_t] + [(p + \tfrac{1}{2}B_\perp^2)u - B_xB_\perp v] = 0, \tag{2.5}$$

where m is defined by $\tau m = u - s$ and s is the shock speed. The specific total energy is given by $e_t = \frac{1}{2}(u^2 + v^2) + \tau p/(\gamma - 1) + \frac{1}{2}\tau B_\perp^2$. The ideal-gas assumption $\tau p = RT$ is applied. $[Q]$ and $\bar{Q}$ denote the jump $Q_R - Q_L$ of a quantity Q and the arithmetic average $\frac{1}{2}(Q_R + Q_L)$ of Q respectively. Subscripts L and R indicate the left state and the right state. *Here the left state and the right state represent properties behind and ahead of the wave respectively.* Note that we use the Lagrangian MHD equations of the variables $(\tau, u, v, B_\perp, p)$. By combining (2.1)–(2.5), (2.5) can be replaced by

$$\left[\frac{\tau p}{\gamma - 1} + \tau\bar{p}\right] + \tfrac{1}{4}[\tau][B_\perp]^2 = 0, \tag{2.6}$$

which is the generalized Rankine–Hugoniot relation first given by Lüst (1955). Note that the case $m = 0$ for non-zero B_x represents a contact discontinuity across which there is only a density jump. Thus we can assume m to be non-zero for shocks. Eliminating $[v]$ and m, we may obtain the Hugoniot relation for the pressure and the transverse magnetic field:

$$\tfrac{1}{4}(\gamma - 1)\bar{B}_\perp[B_\perp]^4 + \tfrac{1}{4}(\gamma - 1)[p][B_\perp]^3 + \gamma\bar{p}\bar{B}_\perp[B_\perp]^2$$

$$+(\gamma\bar{p} - {B_x}^2 - \bar{B}_\perp^2)[p][B_\perp] - \bar{B}_\perp[p]^2 = 0. \tag{2.7}$$

We believe this equation to be new. It can be factored as

$$p_L^2\{\tfrac{1}{2}(\gamma - 1)[B_\perp] - B_{\perp L}\}(Y - Y_1)(Y - Y_2) = 0, \tag{2.8}$$

where $Y = [p]/p_L$ and Y_1, Y_2 are solutions given first by Bazer and Ericson (1958) and Ericson and Bazer (1960). In their notation,

$$Y_{1,2} = \frac{\gamma}{s_L}\left(-\frac{h^2}{2} + h\,\frac{\frac{1}{2}\gamma h\sin\theta_L - 1 + s_L \pm R^{1/2}}{2\sin\theta_L - (\gamma - 1)h}\right), \tag{2.9}$$

where $h, s_L, \sin\theta_L$ and R are defined by

$$h = \frac{[B_\perp]}{(B_x^2 + B_{\perp_L}^2)^{1/2}}, \qquad s_L = \frac{\gamma p_L}{(B_x^2 + B_{\perp_L}^2)^{1/2}}, \qquad \sin\theta_L = \frac{B_{\perp_L}}{(B_x^2 + B_{\perp_L}^2)^{1/2}},$$

$$R = h^2(\tfrac{1}{4}\gamma^2\sin^2\theta_L - \gamma + 1) + h\sin\theta_L(2 - \gamma)(1 + s_L) + 4s_L\sin^2\theta_L + (1 - s_L)^2.$$

https://doi.org/10.1017/S0022377897005941 Published online by Cambridge University Press

Even though the solution (2.9), which treats the left state as a reference, has been the usual basis for MHD shock calculations since the late 1950s, the new relation (2.7), which treats the left and right states symmetrically, is also useful in the sense that it reveals more information on the Hugoniot, for example, asymptotic properties and limiting shocks with zero pressure, and can be readily extended to give the complete solution. For example, given $B_{\perp L,R}$ and $p_{L,R}$ satisfying (2.7), we can derive from (2.6) the density ratio

$$\Omega \equiv \frac{\tau}{\tau_L} = \frac{2\gamma\bar{p} + (\gamma-1)[B_\perp]^2 - 2[p]}{2\gamma\bar{p} + (\gamma-1)[B_\perp]^2 + 2[p]}, \tag{2.10}$$

and subsequently the mass flux via (2.1) and (2.2),

$$|m| = \left(\frac{[p] + \bar{B}_\perp[B_\perp]}{\tau_L(1-\Omega)}\right)^{1/2}. \tag{2.11}$$

Finally, the velocity jumps follow from (2.1) and (2.3).

2.2. MHD shock waves

Whichever method is adopted to find states satisfying the jump relationships, it is necessary to determine which jumps are physically admissible. Some parameters may be found to classify shock types. For a shock, the signs of the following four parameters $P_{1,2,3,4}$ determine which of the magnetoacoustic characteristics run into the shock:

$$c_f - \tau|m|, \qquad \tau|m| - c_s, \qquad c_{f\,L} - \tau_L|m|, \qquad \tau_L|m| - c_s, \tag{2.12}$$

where $c_{f,s}$ are positive propagation speeds satisfying

$$2c_{f,s}^2 = \tau\Big(B_x^2 + B_\perp^2 + \gamma p \pm \{(B_x^2 + B_\perp^2 + \gamma p)^2 - 4B_x^2\gamma p\}^{1/2}\Big),$$

with $c_s \leqslant \tau^{1/2}B_x \leqslant c_f$, and $|m|$ is the absolute value of the mass flow rate. Note that these parameters depend only on p and $B_\perp$.

Similarly to the model studied in Part 1 (Myong and Roe 1997*b*), there are 16 possible sign distributions of these 4 parameters, but only 9 can actually arise, because the following relations must be satisfied:

$$c_s \leqslant c_f, \qquad c_{s\,L} \leqslant c_{f\,L}. \tag{2.13}$$

The classification of shock types is identical with the model. They are slow, fast, slow expansive, fast expansive, overcompressive, undercompressive, expansive, left transport and right transport shocks. At this stage, the classification is merely geometric in nature; we need still to decide which types are physically meaningful. This problem will be treated later in detail.

2.3. Magnetoacoustic rarefaction waves

MHD simple waves, which are rarefaction-wave solutions of the MHD system of equations, have been studied by various researchers. Shercliff (1960) and Mann (1995) examined simple waves in a state space defined as $(\rho, B_\perp)$. Polovin (1961) derived the Riemann invariants in a state space defined as $(a^2/c_a^2,\ c_{f,s}^2/a^2)$. Recently, Roe and Balsara (1996) obtained approximate curves for magnetoacoustic simple waves in a state space $(c_a/a,\ c_{a\perp}/a)$, where $c_{a\perp} \equiv B_\perp\rho^{-1/2}$, starting from the MHD magnetoacoustic eigensystem. Here, we shall follow the approach con-

https://doi.org/10.1017/S0022377897005941 Published online by Cambridge University Press

sidered by Polovin, since it yields an exact relation for MHD simple waves in a monatomic gas.

The system of equations for MHD simple waves can be written as (Jeffrey and Taniuti 1964)

$$-\epsilon c_n\, d\rho + \rho\, du = 0, \tag{2.14}$$

$$-\epsilon c_n \rho\, du + B_\perp\, dB_\perp + a^2\, d\rho = 0, \tag{2.15}$$

$$-\epsilon c_n \rho\, dv - B_x\, dB_\perp = 0, \tag{2.16}$$

$$-\epsilon c_n\, dB_\perp + B_\perp\, du - B_x\, dv = 0, \tag{2.17}$$

with constant B_x and entropy, where the eigenvalue $\lambda = u + \epsilon c_n$. For right-running waves and left-running waves, ϵ is 1 and -1 respectively. Here, c_n, which is the characteristic speed of magnetoacoustic waves, is given by

$$c_n^2 c_{a_\perp}^2 = (c_n^2 - a^2)(c_n^2 - c_a^2). \tag{2.18}$$

From (2.14) and (2.15), we have

$$(a^2 - c_n^2)\, d\rho + B_\perp\, dB_\perp = 0. \tag{2.19}$$

Introducing the variables r and q through

$$r \equiv \frac{a^2}{c_a^2}, \qquad q \equiv \frac{c_n^2}{a^2}, \tag{2.20}$$

we can write (2.18) as

$$B_\perp = \left\{(q-1)\left(r - \frac{1}{q}\right)\right\}^{1/2} \mathrm{sign}(B_x B_{\perp L}). \tag{2.21}$$

From (2.14), we have

$$du = \epsilon c_n \frac{d\rho}{\rho} = \epsilon \frac{c_n}{\rho} \frac{B_x^2}{\gamma a^2}\, dr = \epsilon \frac{c_n}{\gamma} \frac{dr}{r} = \epsilon \frac{a}{\gamma}\, q^{1/2} \frac{dr}{r}, \tag{2.22}$$

where $r = \rho a^2 / B_x^2$ and $c_n = a q^{1/2}$ are used. Thus we derive

$$\frac{du}{dr} = \epsilon \frac{a}{\gamma} \frac{q^{1/2}}{r}. \tag{2.23}$$

From (2.16), (2.17) and (2.21), we have

$$B_x^2 \left(1 - \frac{c_n^2}{c_a^2}\right) dv = \frac{B_\perp}{B_x}\, du \tag{2.24}$$

and finally

$$\frac{dv}{dr} = -\epsilon \frac{a}{\gamma} \frac{\{(q-1)(rq-1)\}^{1/2}}{rq-1} \mathrm{sign}(B_x B_{\perp L}). \tag{2.25}$$

Next, (2.23) and (2.25) can be expressed as

$$\Delta u = \epsilon \frac{\hat{a}}{\gamma} \int q^{1/2}\, r^{-(\gamma+1)/2\gamma}\, dr\,, \tag{2.26}$$

$$\Delta v = -\epsilon \frac{\hat{a}}{\gamma} \mathrm{sign}(B_x B_{\perp L}) \int \frac{\{(q-1)(rq-1)\}^{1/2}}{rq-1}\, r^{-(\gamma+1)/2\gamma}\, dr\,, \tag{2.27}$$

where $\hat{a}^2 = c_{a_L}^2 r_L^{1/\gamma}$. Note that $a^2 = \hat{a}^2 r^{(\gamma-1)/\gamma}$ if we introduce $\hat{\rho}, \hat{p}$ and $\hat{a}$ defined by

https://doi.org/10.1017/S0022377897005941 Published online by Cambridge University Press

$\rho = \hat{\rho} r^{1/\gamma}, p = \hat{p} r$ and $\hat{a}^2 = \gamma \hat{p}/\hat{\rho}$. The relation between r and q in simple waves can be derived by inserting (2.21) and $d\rho = dp/a^2 = (B_x^2/\gamma a^2)\, dr$ into (2.19):

$$\frac{dq}{dr} = \frac{2-\gamma}{\gamma} \frac{q^2(q-1)}{rq^2-1}. \tag{2.28}$$

Direct integration of (2.28) yields the following solution:

$$J = r(q-1)^{-\alpha} + \alpha \int q^{-2}(q-1)^{-(\alpha+1)}\, dq, \tag{2.29}$$

where $\alpha = \gamma/(2-\gamma)$ and J represents the fast and slow magnetoacoustic Riemann invariants. For a monatomic gas, it reduces to the analytic form

$$\begin{aligned} J = {} & \frac{(r-1)}{(q-1)^5} + \frac{5}{2}\frac{1}{(q-1)^4} - \frac{5}{(q-1)^3} + \frac{10}{(q-1)^2} \\ & - \frac{25}{q-1} - \frac{5}{q} + 30 \ln \frac{q}{|q-1|}. \end{aligned} \tag{2.30}$$

For slow waves, $rq-1 < 0, 0 \leqslant q < 1$, whereas $rq-1 > 0, 1 < q < \infty$ for fast waves. The final note is that there exist non-physical portions of rarefaction waves in (r, q) space; from (2.21), it is the region with $(q-1)(rq-1) < 0$, implying that the (r, q) coordinates cannot serve as the final basis for rarefaction waves. In next section, we shall derive the new basis consisting of two non-dimensional parameters.

2.4. Hugoniot curves and integral curves in the reduced plane

For a particular left state, we can use (2.7) or (2.9) to trace the Hugoniot curve. For each state on the curve, we can compute the parameters that describe the characteristic speeds and so identify the shock type corresponding to that point. Based on the relatively simple form (2.7) that the Hugoniot assumes for variables p and $B_\perp$, we choose these variables to represent the phase space, and make them non-dimensional as

$$U = \frac{\gamma p}{{B_x}^2}, \quad V = \frac{B_\perp}{B_x}. \tag{2.31}$$

Then it reduces to

$$([U] + \gamma \bar{V}[V]) \left\{ \gamma(\gamma-1)[V]^3 + 4\gamma \bar{U}[V] - 4\bar{V}[U] \right\} - 4\gamma[U][V] = 0. \tag{2.32}$$

This phase space $\mathbf{U} = (U, V)$ has the advantage of representing MHD waves for non-zero B_x in the sense that

(1) they are non-dimensional parameters by which the umbilic point can be fixed;

(2) they are chosen from the Hugoniot condition, matching the fact that rarefaction waves are the solution of Rankine–Hugoniot relations with the limit of $|\mathbf{u}_R - \mathbf{u}_L| \to 0$;

(3) they can represent the entire physical region defined by $p, \rho, T \geqslant 0$ and $u, v, B_\perp \in \mathbf{R}$.

Neither ρ nor a variable divided by a, for example $(\rho, B_\perp)$ in Shercliff (1960) and Mann (1995), $(a^2/c_a^2,\ c_{f,s}^2/a^2)$ in Polovin (1961) and $(c_a/a,\ c_{a\perp}/a)$ in Roe and Balsara (1996), can define the absolute temperature. Also, $([p]/p_L,\ [B_\perp]/(B_x^2 + B_{\perp_L}^2)^{1/2}$ in Bazer and Ericson (1958) and $(p, B_\perp)$ in Gogosov (1961) do not satisfy

https://doi.org/10.1017/S0022377897005941 Published online by Cambridge University Press

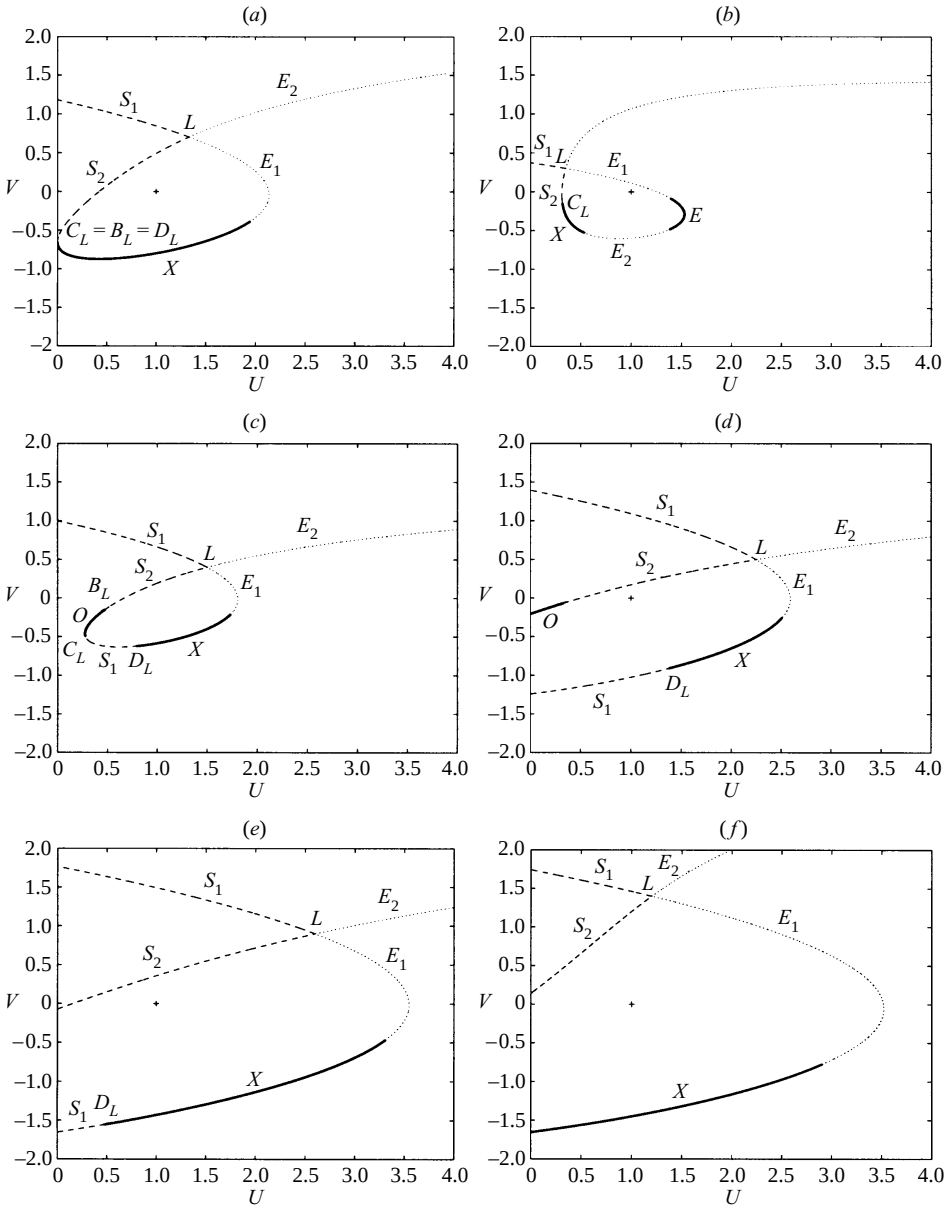


Figure 1. Examples of MHD Hugoniot curves: S_1, S_2, 1, 2 regular; E_1, E_2, 1, 2 expansive; O, X, overcompressive, undercompressive; E, expansive shocks.

property (1). The notation in (2.9) can be expressed in terms of U and V by ($U_L = \gamma p_L/{B_x}^2$, $V_L = B_{\perp L}/B_x$)

$$Y = \frac{U}{U_L} - 1, \qquad h = \frac{V - V_L}{(1 + V_L^2)^{1/2}}, \qquad s_L = \frac{U_L}{1 + V_L^2}, \qquad \sin\theta_L = \frac{V_L}{(1 + V_L^2)^{1/2}}. \quad (2.33)$$

In the (U, V) plane, the shape and classification of the Hugoniot curves is identical for either right-running or left-running waves. Examples of the Hugoniot curves

https://doi.org/10.1017/S0022377897005941 Published online by Cambridge University Press

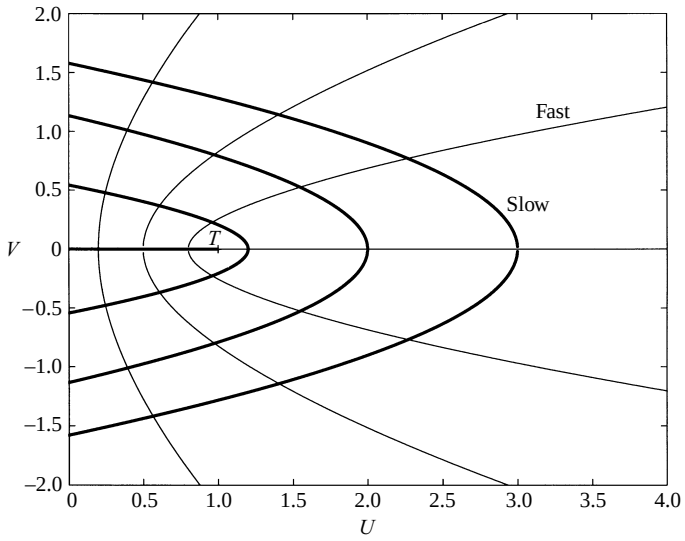


Figure 2. MHD integral curves. The thick solid lines indicate slow rarefaction waves, and the thin lines indicate fast rarefaction waves.

can be found in Fig. 1. Note that all shocks except the transport shocks can be found in the Hugoniot loci of MHD.

Similarly, integral curves defined by (2.30) can be represented by these coordinates using the following relations:

$$r = U, \qquad q = \frac{1}{2U}\left(1 + U + V^2 \pm \{(1 + U + V^2)^2 - 4U\}^{1/2}\right), \tag{2.34}$$

where + and − represent fast and slow waves respectively. Integral curves are depicted in Fig. 2. In Figs 1 and 2, the point $(1, 0)$ is the umbilic point where the slow and fast wave speeds coincide. Figures 1(a–c) are topologically identical to the Hugoniot curves for a particular case of an 2×2 set of conservation laws designed to have a singular point where the wave speeds coincide. The curves have the same general shape as for the model problem, and the various shock types are encountered along them in the same order. In each case, overcompressive shocks are only found if V is sufficiently small. Similarly to the model, the non-convexity of MHD waves is observed, which is illustrated in Fig. 3.

The only structural difference between the model problem and the MHD problem is that in the latter case there is a physical significance to the value $U = 0$, that is, $p = 0$. Thus, for certain positions of the point L, some sections of the Hugoniot may be cut off, as in Figs 1(d–f). The solution of the MHD Riemann problem needs to account for this difference. The effect is to simplify the solution to the Riemann problem for states well away from the umbilic point, and so we will begin with the case where L is close to the umbilic point, and the complete loop to the Hugoniot curve lies in $U > 0$. Then the topology of the Hugoniot and wave curves is identical to that of the model problem.

Specifically, the following shocks are found to be necessary.

(i) *Fast and slow shocks*. These do not change the sign of the transverse field, and are found in Figs 1(a–f) in the upper half-plane, labelled S_1 and S_2.

https://doi.org/10.1017/S0022377897005941 Published online by Cambridge University Press

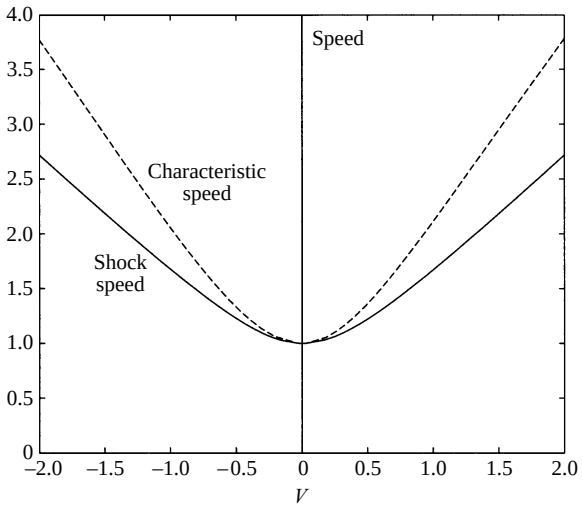


Figure 3. The shock speed and the characteristic speed as a function of V along a MHD fast rarefaction wave with $U_L = 0.5$ and $V_L = 0$.

(ii) *Slow intermediate shocks.* These do change the sign of the transverse field, and are found in Figs 1(*c–e*) in the lower half-plane, labelled S_1.

(iii) *Fast intermediate shocks.* These produce a sign change, and are found in Fig. 1(*a–e*), labelled S_2.

(iv) *Overcompressive shocks.* These produce a sign change, and are found in Fig. 1(c, d), labelled O.

(v) *Transitional cases B_L, C_L and D_L.* These are found in Figs 1(*a–e*).

It should be noted that slow and fast intermediate shocks do not differ from slow and fast shocks in the number of outgoing characteristics in the planar problem. From now on, we call all these shocks slow and fast shocks.

2.5. Admissibility conditions for intermediate shocks

2.5.1. Evolutionary condition. The evolutionary condition developed by Akhiezer *et al.* (1959), Polovin and Demutskii (1990) and Jeffrey and Taniuti (1964) restricts the physically admissible shocks for the planar MHD Riemann problem to planar slow and fast shocks in which the transverse field does not change sign, and the number of small-amplitude outgoing waves is one, equivalent to the number of the boundary conditions minus one ($2 - 1$). It turns out, however, that these shocks alone cannot ensure the uniqueness of the Riemann problem. The failure of the evolutionary condition has become more obvious after several researchers investigated the MHD Riemann problem in numerical experiments (Ugai and Shimizu 1994; Brio and Wu 1988; Kennel *et al.* 1990; Wu 1988*a*, *b*, 1990; Brio and Rosenau 1994). In the past, it was assumed by the evolutionary condition that MHD intermediate shocks are unstable because the linearized perturbation of the jump relations is overdetermined. Contrary to this belief, Brio and Rosenau (1994) showed that the nonlinear intermediate shocks have such characteristics, but the linearized problem cannot be characterized as incoming or outgoing, since there are waves moving with the shock speed.

https://doi.org/10.1017/S0022377897005941 Published online by Cambridge University Press

2.5.2. Viscosity admissibility condition. In the mean time, some mathematicians, working on the Riemann problem of non-strictly hyperbolic conservation laws with application to oil recovery, proposed the viscosity admissibility condition to overcome failure of the evolutionary condition that restricts the characteristics that enter and leave a discontinuity. The viscosity admissibility condition considers relevant discontinuities to be limits of travelling waves for an associated parabolic equation in order to take account of certain physical effects that have been neglected in the ideal equations. Global analysis of the dynamical system defined by travelling-wave solutions to the associated parabolic equation plays a crucial role in this theory. For an example, by applying this criterion to the planar 2×2 model system in case I, Gomes (1989) proved that there are shocks (undercompressive) that have stable viscous profiles but do not satisfy the evolutionary condition. However, these undercompressive shocks are not admissible in the version of the model problem (case IV) that is analogous to MHD.

Therefore we shall adopt the viscosity admissibility condition to determine physically relevant MHD shocks, even though it too can fail to guarantee the existence and uniqueness of the solutions of some Riemann problems (Isaacson *et al.* 1990). The global phase portraits of the planar MHD problem are given in Appendix A. In the finite domain, typically, there are four singularities; two nodes and two saddles. The saddle–saddle connection cannot exist, so undercompressive shocks will be excluded from the wave curve. But overcompressive shocks do have viscous profiles, since a repelling node can be connected with an attracting node. In conclusion, the evolutionary condition excludes certain types of shocks, while the viscosity admissibility condition permits them. It will be shown in Sec. 2.10 that precisely those shocks admitted under the viscosity condition allow unique solutions for all planar MHD Riemann problems.

2.6. Compound waves

Various critical points on the Hugoniot can be identified, where one type of shock gives way to another. The state C_L is the point where the Hugoniot locus is tangent to a fast integral curve. It may be defined as C_L satisfying

$$c_f(\mathbf{U}) - \tau |m(\mathbf{U}_L, \mathbf{U})| = 0. \tag{2.35}$$

From Table 1 in Part 1 (Myong and Roe 1997*b*) it can be found that C_L is on the border between fast shocks and undercompressive shocks or on the border between slow shocks and overcompressive shocks. B_L and D_L may be defined as points satisfying

$$c_s(\mathbf{U}_L) - \tau_L |m(\mathbf{U}_L, \mathbf{U})| = 0. \tag{2.36}$$

Here B_L and D_L are defined for the $+R^{1/2}$ branch and the $-R^{1/2}$ branch at the Hugoniot curve respectively. B_L is on the border between fast shocks and overcompressive shocks, while D_L is on the border between slow shocks and undercompressive shocks.

In order to ensure the uniqueness to the solution, so-called compound waves are introduced as substitutes for undercompressive shocks that are inadmissible by the viscous stability criterion developed in Appendix A. Similarly to the model, they consist of waves of one family (slow or fast), and are of three types.

A slow compound wave C_1 is a slow rarefaction wave R_1 followed by a slow shock S_1. Similarly a fast compound wave C_2 can be defined as a fast shock wave S_2

https://doi.org/10.1017/S0022377897005941 Published online by Cambridge University Press

followed by a fast rarefaction wave R_2. In both cases, the speed of the shock s equals the speed of the adjacent rarefaction wave $u - \mathrm{sign}(m)\, c_{f,s}$. From the definition of critical points (e.g. C_L, B_L and D_L), it can be seen that a slow compound wave C_1 consists of a jump to the point D_L followed by a slow rarefaction R_1, and a fast compound wave consists of a jump to the point C_L followed by a fast rarefaction R_2. Similarly to the model, there is a chance of a slow rarefaction followed by a jump to a fast rarefaction.

2.7. Parallel limit

In the parallel limit ($B_{\perp L} = B_{\perp R} = 0$), the Hugoniot relation becomes

$$\left.\begin{aligned} \frac{[\tau]}{\tau_L} &= -\frac{2[p]}{(\gamma+1)[p] + 2\gamma p_L}, \\ \text{with} \qquad m &= -\frac{[p]}{[u]} = \frac{[u]}{[\tau]},\ m^2 = -\frac{[p]}{[\tau]}. \end{aligned}\right\} \tag{2.37}$$

The signs of the four parameters P_1, P_2, P_3 and P_4 can be determined by

$$\{\gamma(1 + U_R + |1 - U_R|)\}^{1/2} - \{(\gamma+1)U_L + (\gamma-1)U_R\}^{1/2}, \tag{2.38}$$

$$-\{\gamma(1 + U_R + |1 - U_R|)\}^{1/2} + \{(\gamma+1)U_L + (\gamma-1)U_R\}^{1/2}, \tag{2.39}$$

$$\{\gamma(1 + U_L + |1 - U_L|)\}^{1/2} - \{(\gamma-1)U_L + (\gamma+1)U_R\}^{1/2}, \tag{2.40}$$

$$-\{\gamma(1 + U_L + |1 - U_L|)\}^{1/2} + \{(\gamma-1)U_L + (\gamma+1)U_R\}^{1/2}. \tag{2.41}$$

Using the shock theory developed in Sec. 2.2, we can classify all parallel shocks:

$$S_1 - E_1 - E - E_2 \quad \text{if } 0 < U_L < 1, \tag{2.42}$$

with boundary points U_L, U', U'', where

$$U' \equiv \frac{2\gamma}{\gamma+1} - \frac{\gamma-1}{\gamma+1}U_L, \quad U'' \equiv \frac{2\gamma}{\gamma-1} - \frac{\gamma+1}{\gamma-1}U_L;$$

$$S_1 - O - S_2 - E_2 \quad \text{if } 1 < U_L < \frac{2\gamma}{\gamma+1}, \tag{2.43}$$

with boundary points U'', U' and U_L;

$$O - S_2 - E_2 \quad \text{if } \frac{2\gamma}{\gamma+1} < U_L < \frac{2\gamma}{\gamma-1}, \tag{2.44}$$

with boundary points U' and U_L;

$$S_2 - E_2 \quad \text{if } \frac{2\gamma}{\gamma-1} < U_L, \tag{2.45}$$

with a boundary point U_L. In the second case, S_1 and O meet at a particular point defined by

$$U_{C_L} = \frac{2\gamma}{\gamma-1} - \frac{\gamma+1}{\gamma-1}U_L. \tag{2.46}$$

Note that

$$\lim_{U_L \to 1} U_{C_L} = 1. \tag{2.47}$$

https://doi.org/10.1017/S0022377897005941 Published online by Cambridge University Press

Also, rarefaction waves in the parallel limit can be derived from (2.14)–(2.17). They yield

$$(a^2 - {c_n}^2)\, d\rho = 0, \qquad du = \epsilon c_n \frac{d\rho}{\rho}, \qquad dv = dB_\perp = 0, \tag{2.48}$$

and become

$$\Delta u = \epsilon \int \frac{a}{\rho}\, d\rho, \tag{2.49}$$

which is the solution of a pure gas rarefaction wave. It can be rewritten in our (U, V) space, noting that $da/a = (\gamma - 1)/2(d\rho/\rho)$,

$$J = u - \epsilon \frac{2a}{\gamma - 1}. \tag{2.50}$$

Along pure gas rarefaction waves, the velocity u is determined solely by the pressure, yielding the so-called p–u diagram.

$$\Delta u = \epsilon \frac{2}{\gamma - 1} \frac{|B_x|}{\rho_L^{1/2}} U_L^{-1/\gamma} \int U^{(\gamma+1)/\gamma}\, dU, \tag{2.51}$$

since $a = |B_x|/\rho_L^{1/2}(U/U_L)^{1/\gamma} U$.

2.8. Non-classical wave mechanisms

Up to now, we have developed the theory on nonlinear MHD waves to solve the piston problem in which only one of the left and right states, together with the state between the slow waves is considered. Even the solution to this restricted Riemann problem involves 17 different cases. Each wave, fast and slow, may be a regular shock, a compound wave or a rarefaction wave, or it may be absent. The 17th case is where the fast and slow shocks coalesce into an overcompressive shock. Which of these cases occurs will depend on where the left and right states lie with respect to certain critical curves, which will now be described.

Five critical curves are plotted in Fig. 4(*a*). They are explained in Appendix B. The figure shows shock-wave mechanisms available to change the sign of the transverse field. The PC^*U^* critical curve is shown by dotted lines, because it is not critical in shock-wave mechanisms. Each region enclosed by four critical curves ($TC^*, C^*U^{**}, C^*\infty$ and PU^{**}) will have certain shocks available to change the sign. There exist five different cases: $S_1, S_2, S_1S_2, S_1S_2O$ and no shock. All properties are symmetrical about the $V_L = 0$ axis. Points marked as + represent the reference states in Figs 1(*a*–*f*).

Compound waves can also change the sign. Slow compound waves C_1 are available everywhere, but fast compound waves C_2 are available only when the critical point C_L exists. Whether C_L exists for a particular reference state can be determined by checking C_L for intermediate states that move along the slow shock S_1 and the slow integral curve R_1 originating from the reference L. By this procedure, we can find the region in which fast compound waves C_2 are available, which is illustrated in Fig. 4(*b*). The region is enclosed by the boundary that consists of some parts of the PC^*U^* critical curve and a section of the slow integral curve starting at C^*. Some curves are shown by dotted lines to explain how the boundary (indicated by solid lines) is determined. Note that fast compound waves are available where L is close to the umbilic point.

Finally, by combining shock- and compound-wave mechanisms, it can be shown that MHD wave mechanisms have eight different cases, which is illustrated in Fig. 5.

https://doi.org/10.1017/S0022377897005941 Published online by Cambridge University Press

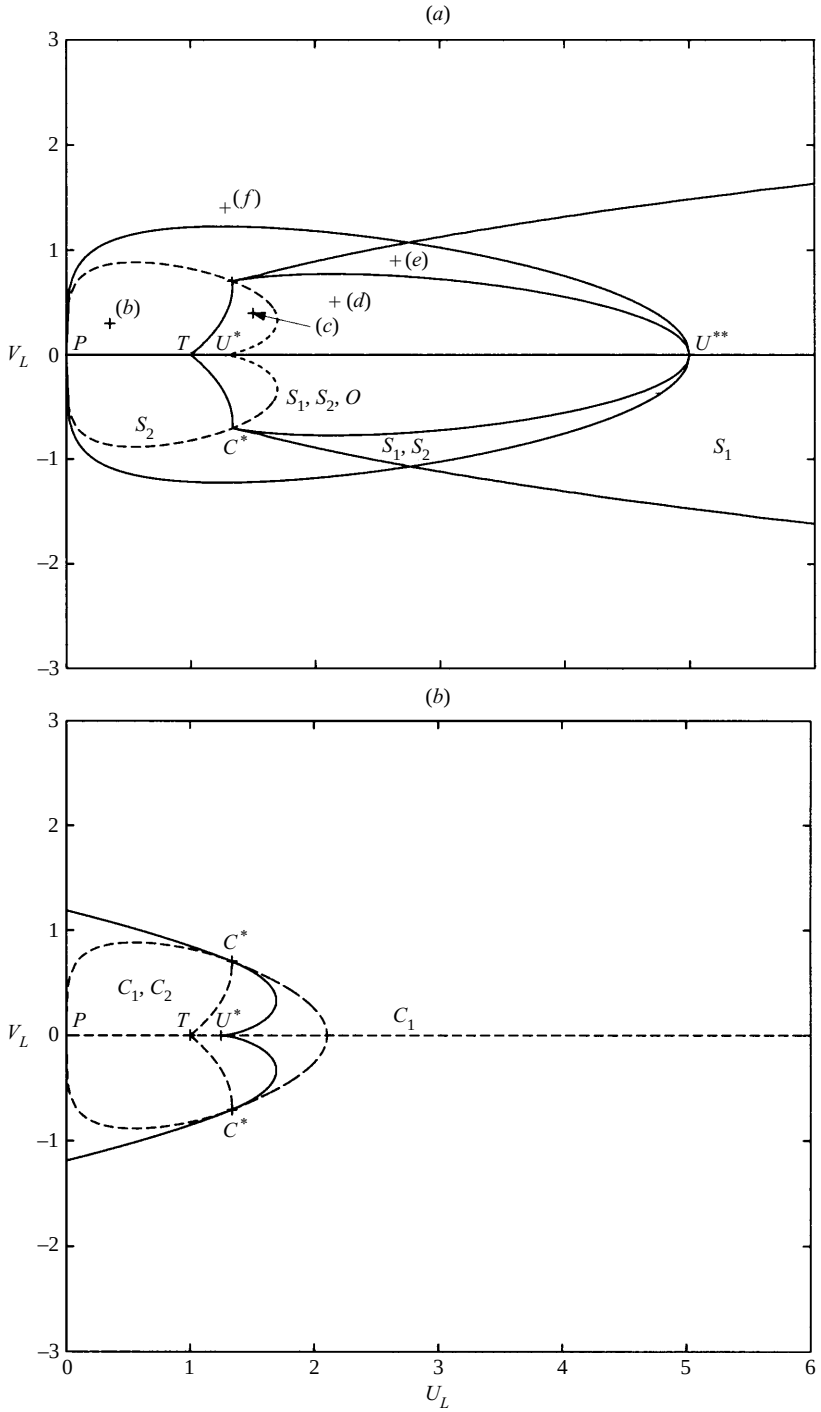


Figure 4. (*a*) Shock mechanisms available to change the sign of the transverse field: the PC^*U^* critical curve is indicated by dotted lines, while the others are indicated by solid lines. (*b*) Compound-wave mechanisms available to change the sign: fast compound waves are available within the boundary curve indicated by solid lines. T and P represent the umbilic point and the origin respectively.

https://doi.org/10.1017/S0022377897005941 Published online by Cambridge University Press

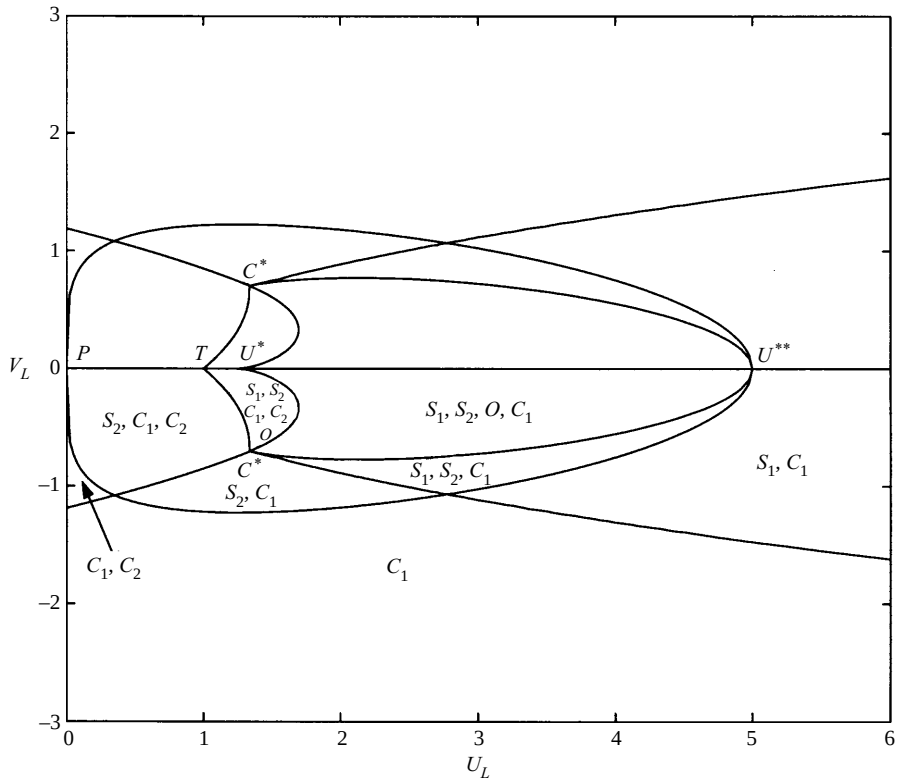


Figure 5. MHD mechanisms available to change the sign of the transverse field: critical curves are shown by thin solid lines. Waves available to change the sign are indicated in the lower half-plane. All properties are symmetrical about the U_L axis.

2.9. Switch-on and switch-off waves

In MHD, switch-on waves are defined as shocks or rarefaction waves by which the transverse magnetic field is generated at the expense of a decrease in pressure. Because in our formulation the left state represents properties behind the wave, such waves are those satisfying $V_R = 0$ and $V_L \neq 0$. Among slow and fast waves, slow rarefaction waves and fast shocks can produce the magnetic field. For slow rarefaction waves, the possible region in (U, V) space can be defined as any U_L on slow integral curves starting from U_R, satisfying $U_L < U_R$ and $U_R > 1$. For fast shocks, only U_L within the region enclosed by the PU^{**} critical curve can have the corresponding right state U_R restricted by $0 \leqslant U_R < 1$, for which $V_R = 0$.

On the other hand, switch-off waves are defined as shocks or rarefaction waves for which the transverse magnetic field vanishes. That is, all the magnetic energy vanish, causing an increase in the thermal energy. Such waves are those satisfying $V_L = 0$ and $V_R \neq 0$. In contrast to switch-on waves, for slow shocks and fast rarefaction waves, the magnetic field can vanish in crossing over waves. For fast rarefaction waves, the possible region is defined as any U_R on fast integral curves starting from U_L satisfying $U_L < U_R$ and $U_L < 1$. For slow shocks, U_R within the region defined by the Hugoniot curve passing through the point $(U^*, 0)$ can have the corresponding switch-off state satisfying $1 < U_L < U^*$. U_R outside the region can also have the corresponding switch-off state satisfying $U^* < U_L$.

https://doi.org/10.1017/S0022377897005941 Published online by Cambridge University Press

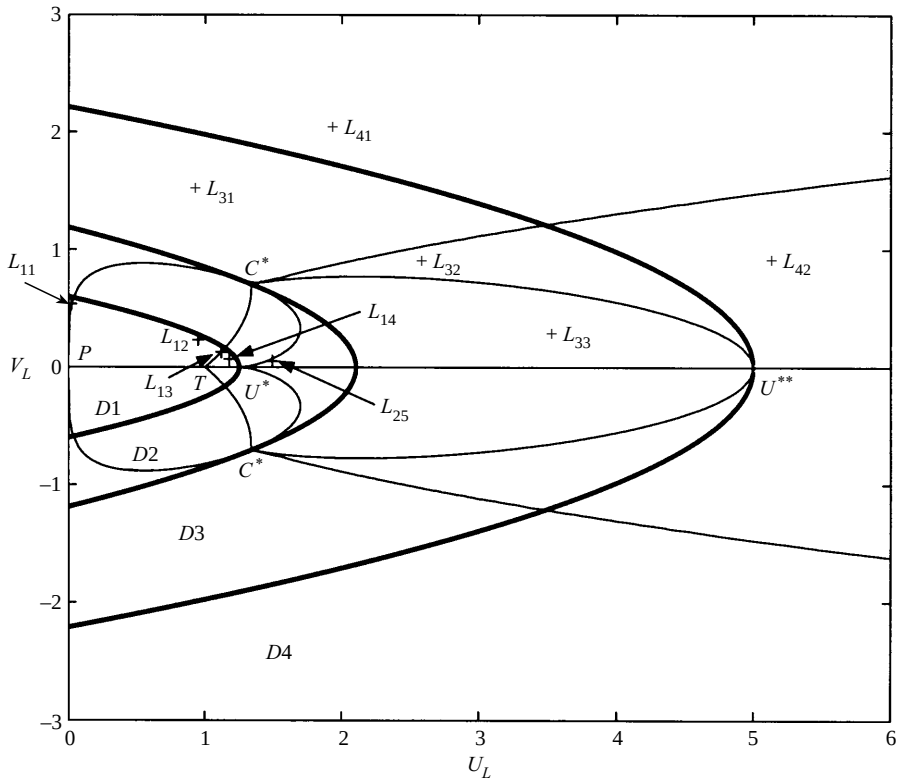


Figure 6. Classification of domains by wave combinations and solution patterns. Critical curves are shown by thin solid lines, while slow integral curves are shown by thick solid lines. The reference states can be classified into four subdomains $D1, D2, D3$ and $D4$. The left states ($L_{11} - L_{42}$) that represent the reference state in sectors are marked by +.

2.10. Solution of the piston problem

The solution of the Riemann problem in (U, V) space consists of a path LIR, where L and R are the given left and right states and I is an intermediate state such that LI is a valid slow wave and IR is a valid fast wave. To facilitate this construction, we define the wave curve associated with a given left state L as the set of all points that can be reached from L by valid waves. These comprise all points on the Hugoniot through L representing valid shocks, all points on the integral curves through L representing valid rarefaction waves, and all points that can be reached from L through compound waves. Then I lies on the wave curve through L, and R lies on the wave curve through I.

For a given left state, a right state will be connected by one of 17 different wave combinations. Therefore there may exist a large number of cases in solution patterns that will be beyond classification. However, thanks to the classification of MHD wave mechanisms available to change the sign, we can classify left states into some subdomains in which the solution patterns are qualitatively the same. These subdomains will be defined in the next section.

2.10.1. Classification of domains by wave combinations and solution patterns. Which MHD waves are available to change the sign, as described in Fig. 5, will play a

https://doi.org/10.1017/S0022377897005941 Published online by Cambridge University Press

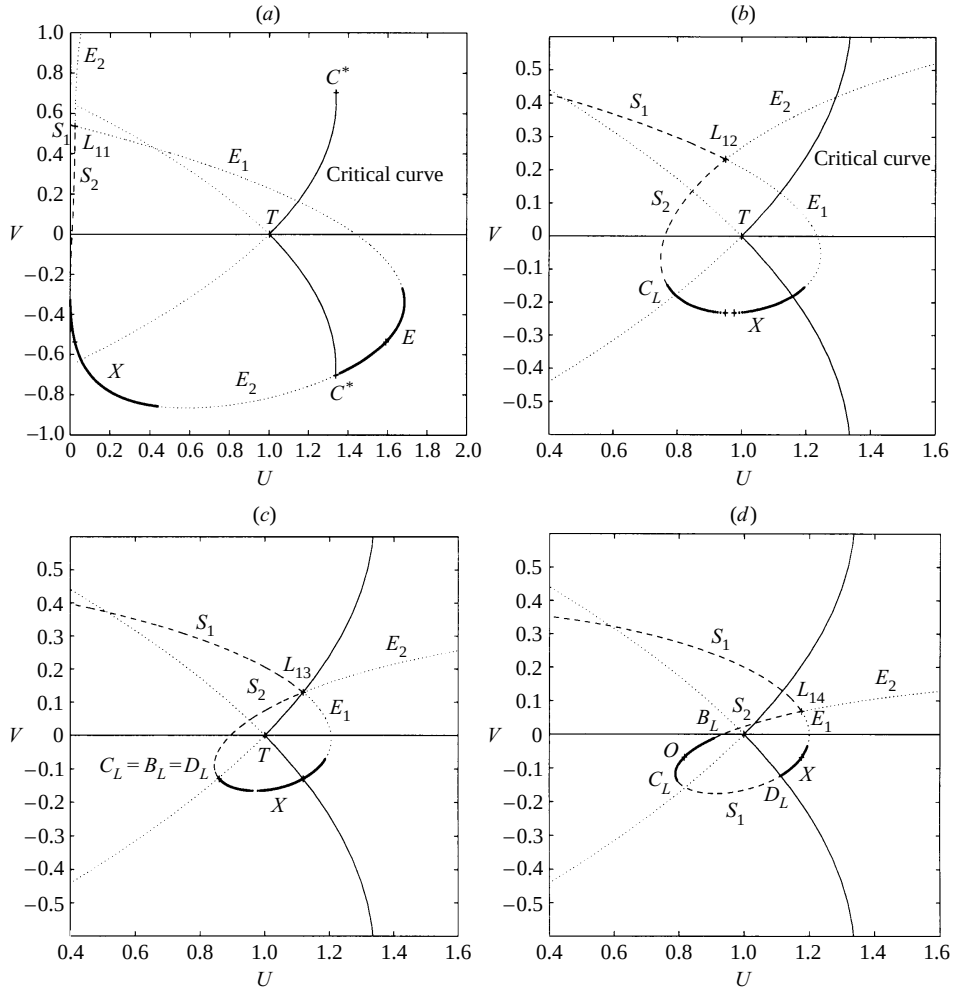


Figure 7. MHD Hugoniot loci and shock types in the domain $D1$: S_1, S_2, 1, 2 regular; E_1, E_2, 1, 2 expansive; E, expansive; O, overcompressive; X, undercompressive shocks.

crucial role in classifying domains by wave combinations. But the PU^{**} curve in Fig. 5 is not critical for wave combinations, even though it is critical for wave mechanisms changing the sign. Thus it will not be considered in classifying domains by wave combinations. The only remaining criterion for the classification of domains is the slow integral curve. The reason for this is that for a left state, different wave combinations begin to appear as intermediate states move along the slow integral curve. Therefore, *by inserting slow integral curves passing U^*, C^* and U^{**}, four subdomains can be defined.* These subdomains are shown in Fig. 6. In each subdomain, the solution is different in sectors 2–4. Note that sectors are defined by which wave combinations exist, and subdomains are defined by the set of such sectors. In order to show the solution in each sector, nine cases (L_{11}, $L_{12}, L_{14}, L_{25}, L_{31}, L_{32}, L_{33}, L_{41}, L_{42}$) marked as + in Fig. 5 will be considered. L_{11} represents a left state in the first sector of subdomain $D1$. A special case L_{13} will be considered to show the transition between the solution of case L_{12} and the solution of case L_{14}. Note that L_{21}, L_{22}, L_{23}

https://doi.org/10.1017/S0022377897005941 Published online by Cambridge University Press

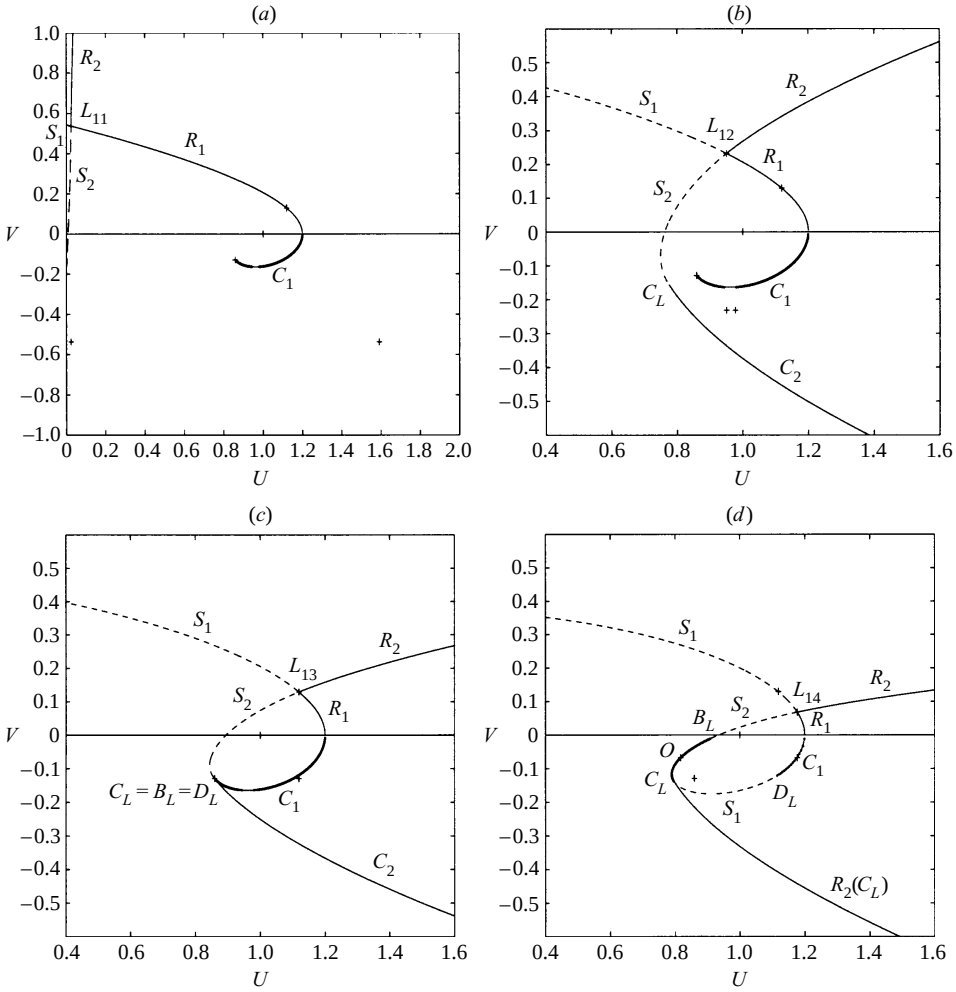


Figure 8. MHD wave curves in the domain $D1$: C_1, C_2, 1, 2 compound waves. $R_2(C_L)$ represents a fast rarefaction wave curve originating from the point C_L.

and L_{24} are not considered. The reason for this is that because the critical points B_L and D_L on the Hugoniot of the left states of first three sectors in subdomain $D2$ always exist, the pattern of wave combinations is the same as that of subdomain $D1$.

Now we shall construct the solution to the Riemann problem. This construction can be explained with the help of Figs 7 and 8. Figures 7(*a–d*) show that Hugoniot curves in the domain $D1$ may be classified into two cases. For reference states L_{11} and L_{12} that are located on the left of the critical curve TC^*, there are no overcompressive shocks or slow shocks with negative V. However, both shocks can be found for L_{14}. Thus this difference in admissible shock curves has an important effect on the solution of the Riemann problem. Once integral curves and Hugoniot loci and compound waves are given for a particular left state, the wave curves are the set of waves: 1, 2 rarefaction waves; 1, 2 shock waves; 1, 2 compound waves; and fast rarefaction wave originating from point C_L. These wave curves in the domain $D1$ are shown in Fig. 8. Points marked as + represent left state, umbilic point, the

https://doi.org/10.1017/S0022377897005941 Published online by Cambridge University Press

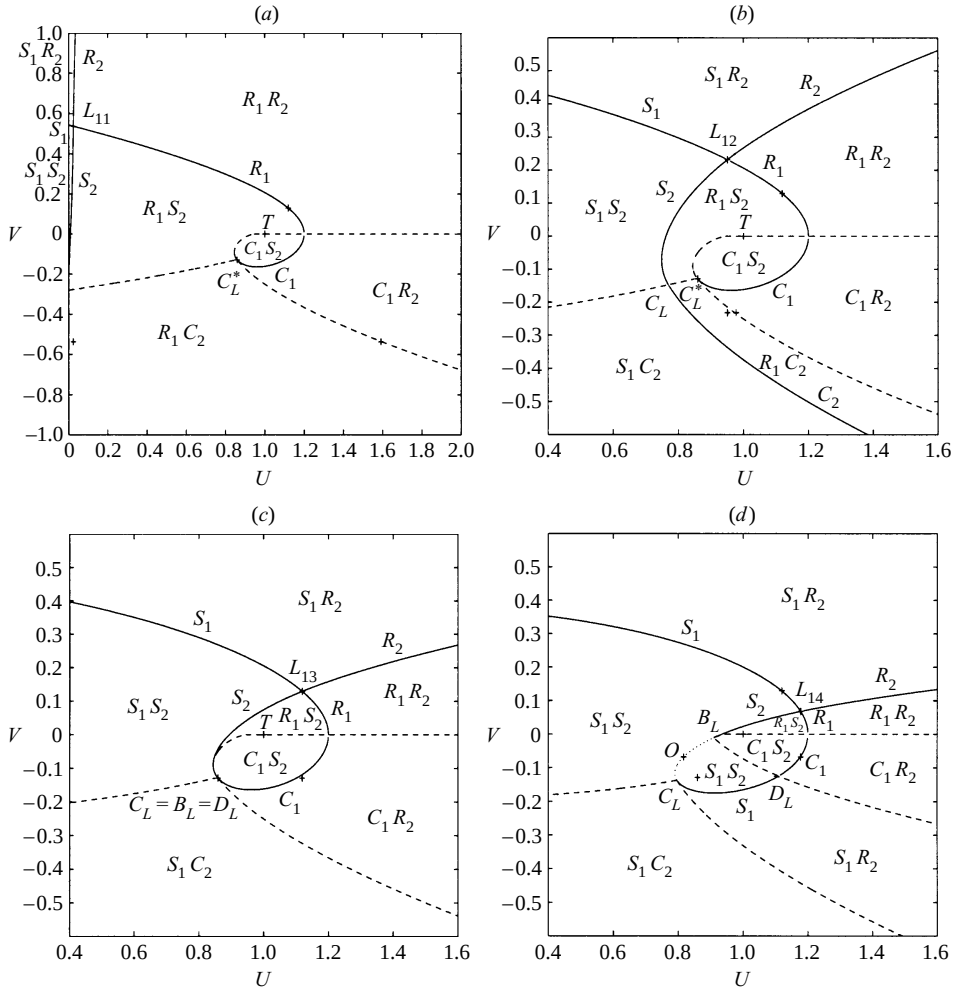


Figure 9. MHD Riemann problem solution in the domain $D1$: solid line, boundary line across which one wave is zero; dashed line, one wave changes character; dotted line, no change.

reflection points of left states including one on TC^* curve (i.e. $[U] = \bar{V} = 0, \bar{V} = 0$), and U_R from (B 6).

We now discuss all four cases, including the switch-off shock solution and the parallel-shock solution.

2.10.2. Solution for subdomain $D1$. Figures 9(a–d) and 12(a, b) comprise the full set of solutions by which all possible cases can be represented. In Fig. 9(b), the left state is located above the critical curve TC^*. The overcompressive shocks and slow shocks cannot be found below the U axis. There are three dotted curves, splitting at the point C_L^*. The curve $\{-\infty C_L^*\}$ is the boundary curve on which the fast shock becomes the fast compound wave. The curve $\{C_L^*\infty\}$ represents fast rarefaction waves on which the solution is the limit of either C_1R_2 or R_1C_2. If the right state is on this curve, the solution is C_1C_2 or R_1R_2. The curve $\{C_L^*T\}$ is the set of locus B_L as the intermediate state moves along the slow rarefaction-wave

https://doi.org/10.1017/S0022377897005941 Published online by Cambridge University Press

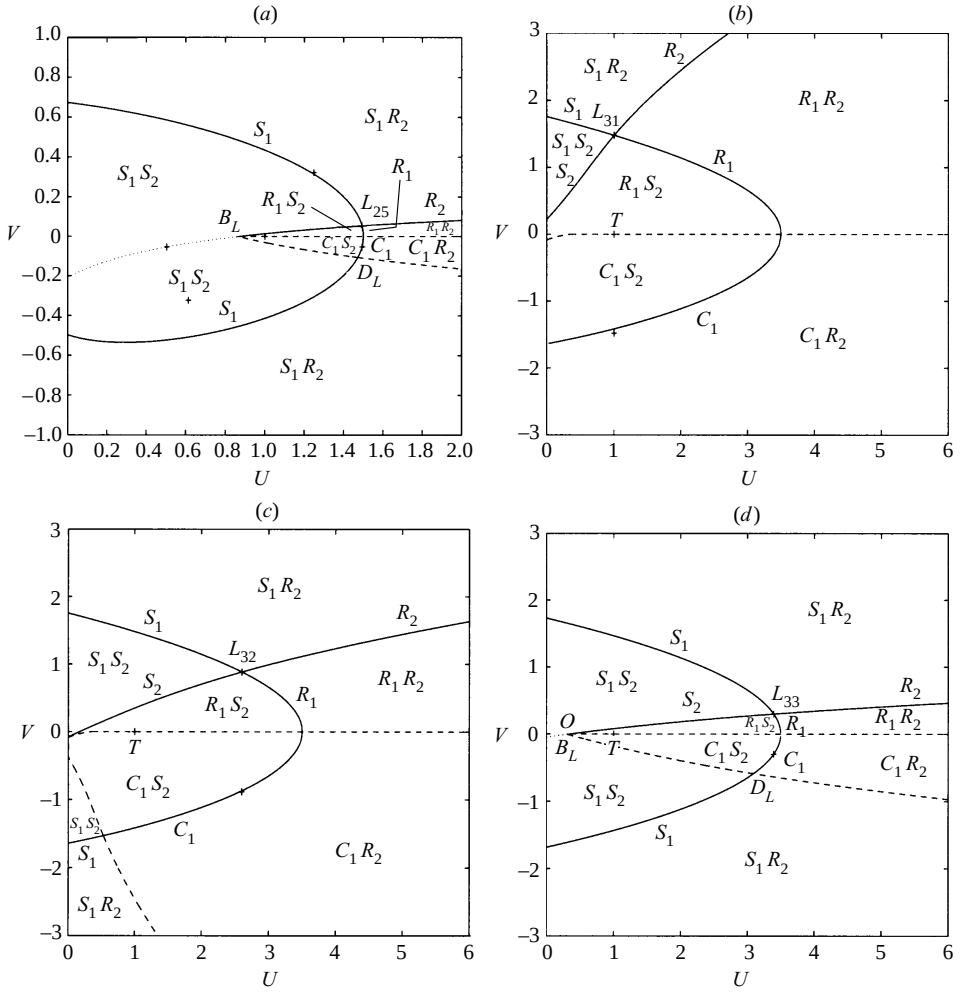


Figure 10. MHD Riemann-problem solution: (*a*) in the domain $D2$ and (*b–d*) in the domain $D3$.

curve. It is the boundary of R_1S_2 and C_1S_2, which represent two different paths. In fact, two solutions are identical in the physical space (x, t) owing to equal shock speed, and are called a *triple shock* (Isaacson 1988*a*, *b*). Note that right states that are connected by compound waves always exist below the U axis. In Figs 9(*c*, *d*), the point C_L begins to bifurcate three points B_L, D_L and C_L itself. Overcompressive shocks emerge as the triple shock region $\{B_LT\}$ shrinks. The solution S_1R_2 can be found below the axis due to the presence of slow shocks, while the solution R_1C_2 disappears. The configuration of solutions becomes symmetrical as the left state approaches the axis. Figures 12(*a*, *b*) show switch-off shocks and parallel shocks in domain $D1$. In Fig. 12(*b*), overcompressive shocks are observed on the line $\{C_LB_L\}$. We can clearly see the continuous dependence of solutions on the left state.

2.10.3. Solution for subdomain D2. Figure 10(*a*) in addition to Figs 9(*a–d*) and 12(*c*) comprise the full set of solutions in domain $D2$. The only difference with domain $D1$ comes with opening from the closed Hugoniot loci near the $V = 0$ axis due

https://doi.org/10.1017/S0022377897005941 Published online by Cambridge University Press

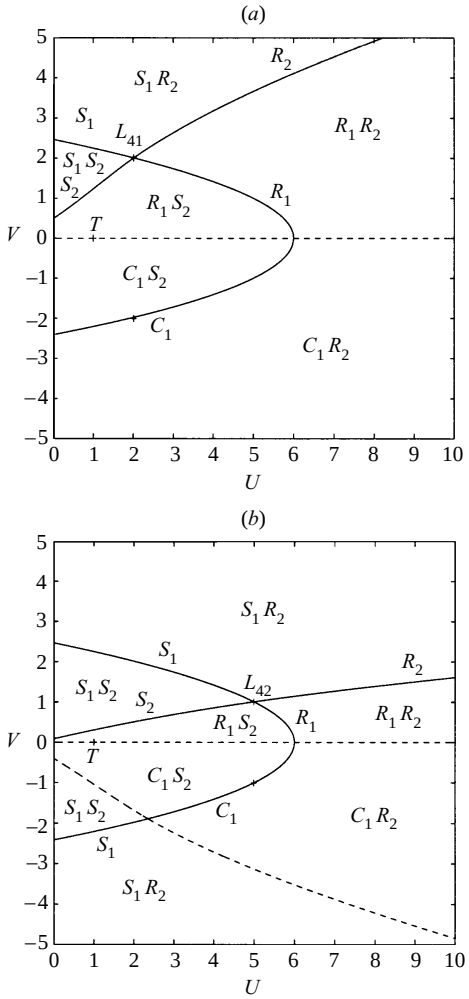


Figure 11. MHD Riemann problem solution in the domain $D4$.

to negative pressure. As a result, fast compound waves become lost in the domain as the left state approaches the axis. In contrast to domain $D1$, the zero-pressure state can be obtained by overcompressive shocks and S_1R_2 combinations.

2.10.4. Solution for subdomain D3. Figures 10(*b–d*) and 12(*c*) comprise the full set of solutions in domain $D3$. Figures 10(*b–d*) represent solutions in three subdomains separated by two critical curves, C^*U^{**} and $C^*\infty$. The distinctive feature is that some parts are always cut out of the Hugoniot loci loop owing to the zero-pressure limit. As the left state moves, slow shocks with opposite sign begin to emerge in advance of overcompressive shocks. As a result, fast compound waves disappear in domain $D3$, and a new C_1S_2 combination can make the right state reach absolute temperature or zero pressure.

2.10.5. Solution for subdomain D4. Figures 11(*a, b*) and 12(*c*) comprise the full set of solutions in domain $D4$. The presence of a critical curve yields two cases in the pattern of solution. The solution is almost the same as that in domain $D3$.

https://doi.org/10.1017/S0022377897005941 Published online by Cambridge University Press

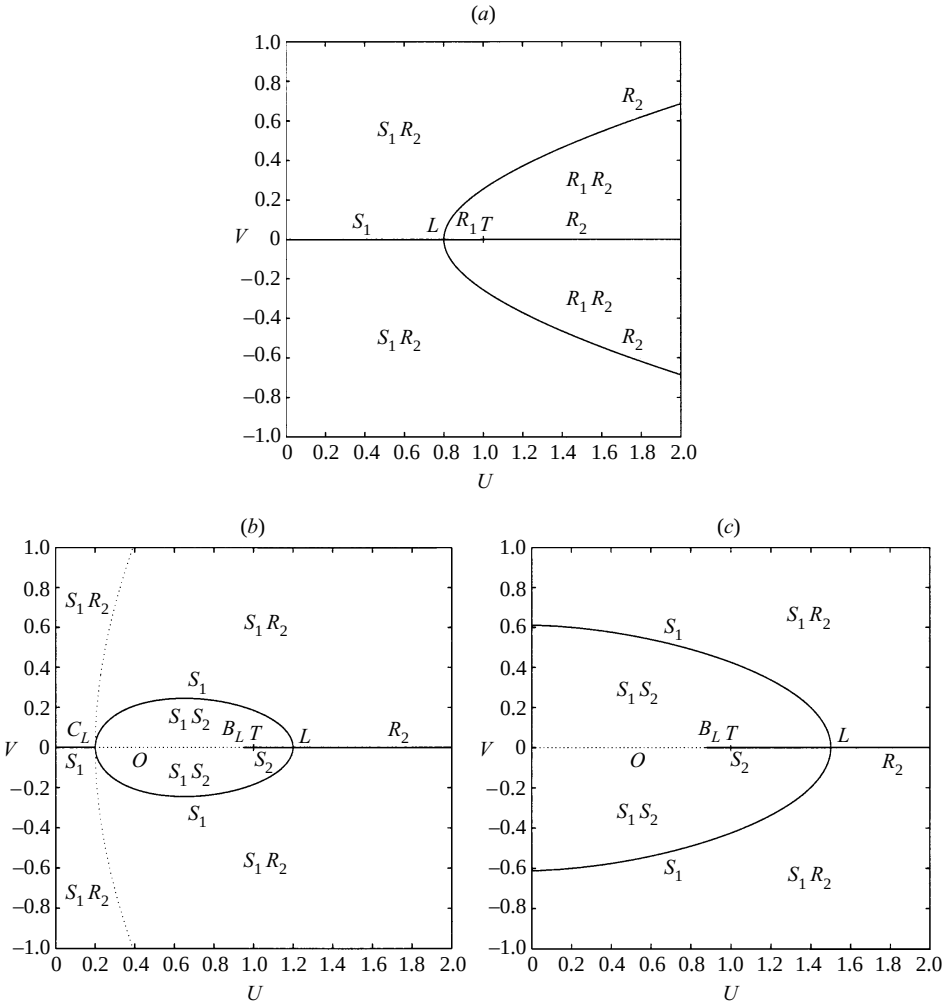


Figure 12. MHD switch-off and parallel-shock solution: (*a*) $U_L < 1$; (*b*) $1 < U_L < U^*$; (*c*) $U^* < U_L$.

However, a case corresponding to Fig. 10(*d*) cannot be found, owing to the absence of overcompressive shocks. In Figs 11(*a*, *b*), it can be observed that the U axis itself is a boundary line across which one wave changes character.

2.10.6. Solutions requiring special waves. Figures 12(*a–c*) represent all the possible solutions for switch-off shocks and parallel shocks. Switch-off shocks can be calculated by substituting $V_L = 0$ into (2.9), and parallel shocks are given in Sec. 2.7. When $U_L < 1$, switch-off can be accomplished only by the fast rarefaction wave. As U_L passes the umbilic point, switch-off shocks begin to emerge. Switch-off can be obtained only through the slow shock, as shown in Figs 12(*b*, *c*). It can be shown from Figs 9–12 that switch-on and switch-off can be attained only through R_1, S_2 and S_1, R_2 respectively.

Finally, we have described all possible wave combinations and mechanisms chang-

https://doi.org/10.1017/S0022377897005941 Published online by Cambridge University Press

ing the sign. It is shown that solutions in domains $D1$ and $D2$ are most general, in other words most complicated, and are almost the same as that of the 2×2 model system. Solutions in domains $D3$ and $D4$ have the same features, but, owing to the cutting off of the Hugoniot locus by the zero-pressure limit, they become different. It is also shown from solution diagrams that the viscosity admissibility condition has the advantage of ensuring the existence and uniqueness of solutions over the evolutionary condition. On the other hand, the evolutionary condition cannot ensure the existence of solutions when all non-evolutionary solutions are strictly excluded. This can be manifested by considering a case in the parallel limit. From Figs 12(b, c), it can be observed that the solutions involve overcompressive shocks, and thus there does not exist any evolutionary solution. In fact, the evolutionary condition is not different from ignoring all shocks with opposite sign for V. Therefore, within its framework, all overcompressive shocks, compound waves, and slow, fast intermediate shocks are lost.

3. Non-planar MHD system

One of the important consequence of the study of the 3×3 non-planar model Riemann problem is that for given left and right states the evolution of waves is highly nonlinear and sometimes may undergo an abrupt change in configuration, depending on the transverse field moment, even though all such time-dependent phenomena will disappear at the very large time. Since many interesting phenomena arising in plasmas, for example, magnetic substorms, and disruptive processes in thermonuclear fusion reactors, are inherently time-dependent problems, we expect that the investigation of the nonlinear evolution of finite-amplitude waves is of critical importance.

In general, there are several effects that may add essential modifications to the nonlinear evolution of waves. All are related to the modification of $\int_{-\infty}^{\infty} \mathbf{u}\, dx$. These are of two types: a self-consistent driving mechanism and external disturbances. In Part 1 (Myong and Roe 1997*b*), we discussed how finite-amplitude waves develop nonlinearly when they are subject to disturbances. For the problem of drivers, a substantial literature exists, even though this is mostly limited to models approximating only rotational singularity (Hada *et al.* 1993). In this section, we study the relationship between the model and the MHD system.

The physical and mathematical reasoning for approximating a 7×7 MHD system by a 3×3 model system rests on the surprising simplicity of MHD system, where MHD waves are symmetric about the contact discontinuity, which always moves with the fluid particles. Therefore, when $c = \gamma + 1$ and the reference states of the MHD Riemann problem lie near the umbilic point, the behaviour of waves found in the model system and the MHD system is identical. The correspondence between the two systems can be summarized as follows:

$$\text{variable} \quad u \qquad U - 1; \tag{3.1}$$

$$\text{variable} \quad v \qquad \frac{B_y}{B_x}; \tag{3.2}$$

$$\text{variable} \quad w \qquad \frac{B_z}{B_x}; \tag{3.3}$$

$$\text{energy} \quad \tfrac{1}{2}(u^2+v^2+w^2) \qquad \frac{p}{\gamma - 1} + \frac{{B_y}^2 + {B_z}^2}{2}; \tag{3.4}$$

https://doi.org/10.1017/S0022377897005941 Published online by Cambridge University Press

entropy-flux condition	$[u] < 0$	$[p] < 0$;	(3.5)
shock speed	s	τm;	(3.6)
parameters	$\lambda_{f,a,s} - s$	$c_{f,a,s} - \epsilon\tau m$;	(3.7)
critical curves	$v = \pm c^{1/2}u$	TC^*.	(3.8)

Notice that $p/(\gamma - 1) + \frac{1}{2}(B_y^2 + B_z^2)$ is an essential energy, since the velocity and the density profiles in the Riemann problem depend on the pressure and the magnetic-field profiles.

In conclusion, all the properties (Hugoniot curve, integral curve, critical curve and point, shock types, eigensystem, and solution patterns) are the same. Differences are found only in limiting cases: vacuum, and absolute temperature limits.

Therefore most results on the evolution of MHD shock waves developed from the model can be applied without alteration to the MHD system. In particular, the theory of the stability of intermediate shocks will also be valid in MHD. That is, intermediate shocks are unstable under any non-coplanar variations of the upstream and downstream states, so that the large-time solution contains only regular shocks. However, in the coplanar problem, they can survive. Even under coplanar variation, they may be expected to decay slowly, so that they are needed to explain small-time and intermediate-time behaviour.

4. Concluding remarks

In this paper, we have proposed a method for classifying magnetohydrodynamic shocks. This method requires shock relations in Lagrangian description and new exotic shocks. On the basis of this method, we construct the solution to the planar Riemann problem on one-directional waves in MHD. In this solution, all the complicated waves are classified under a unified framework. It is also shown that solutions can be characterized by the subdomains in which the reference state lies. These subdomains are determined by checking the existence of overcompressive shocks and slow shocks available to change sign and also by investigating switch-on shocks and parallel shocks. The solution is most complicated in subdomains $D1$ and $D2$, and is almost the same as that of the model system. The transverse magnetic field can change the sign through overcompressive shocks and slow, fast intermediate shocks – some of which belong to compound waves. Moreover, we demonstrate that the difference between solutions in the four subdomains is caused by the cutting off of the closed Hugoniot locus by the zero-pressure state. In addition, by investigating the configuration of singularities of MHD shocks, we show that undercompressive shocks have to be excluded in constructing the planar Riemann solution. Although the Riemann solution is obtained for one-directional waves, analytical results can yield interesting information on understanding the complicated behaviour of MHD shocks and rarefaction waves.

For the general case of the Riemann problem involving left-running and right-running waves, the well-posedness of the problem was proved in Myong and Roe (1997*a*). The final result is that the correspondence of the Riemann data $(\tau_{l,r}, p_{l,r}, B_{\perp l,r}, \Delta u, \Delta v)$ to a set of three arbitrary points in $\mathbf{U}$ phase space is one-to-one. Therefore all previous numerical solutions of the MHD planar Riemann problem can be explained by our analytical solutions. For example, for MHD Sod's test problem (Brio and Wu 1988), we can show that for left-running waves the

https://doi.org/10.1017/S0022377897005941 Published online by Cambridge University Press

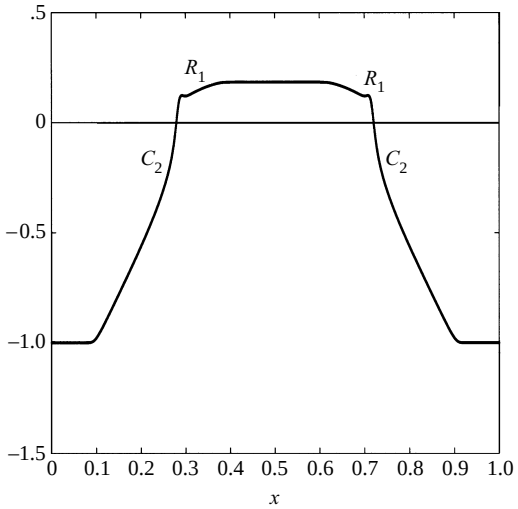


Figure 13. An example of the MHD Riemann problem involving a double change in the sign of $B_\perp$. The vertical axis measures the magnetic field $B_\perp$.

intermediate state belongs to the domain $D3$, and its solution is a fast rarefaction wave followed by a slow compound wave. In addition, nonlinear interaction of MHD discontinuity, for example, the heliospheric termination shocks (Naidu and Barnes 1994) and the merging of compressive waves (Whang 1996) can be explained within the framework of this study. Interestingly, for a case with same sign of magnetic field in the full Riemann problem, an intermediate state separated by a contact discontinuity can be located in the region with opposite sign, depending on given velocity differences. For example, the Riemann solution for Riemann data $\rho_{l,r} = p_{l,r} = 1, B_{\perp l,r} = -1$ and $\Delta u = \Delta v = 2.5$ with $\gamma = \frac{5}{3}$ and $B_x = 1$ involves symmetric intermediate shocks embedded in fast compound waves, which are illustrated in Fig. 13.

Acknowledgements

This work was supported in part by the National Science Foundation under Research Grant ATM-9318181. Also, R.S.M. wishes to thank the Korean Ministry of Education for its financial support in the initial stage of his graduate studies at the University of Michigan.

Appendix A. Analysis of the MHD dynamical system

A.1. The MHD dynamical system

The MHD dynamical system can be derived from the non-ideal MHD equations, which are obtained by adding viscous terms to the ideal MHD equations.

$$\begin{pmatrix} \tau \\ u \\ v \\ \tau B_\perp \\ e_t \end{pmatrix}_{t'} + \begin{pmatrix} -u \\ p + \frac{1}{2}B_\perp^2 \\ -B_x B_\perp \\ -B_x v \\ (p + \frac{1}{2}B_\perp^2)u - B_x B_\perp v \end{pmatrix}_{\xi} = \begin{pmatrix} 0 \\ \mu u_x \\ \nu v_x \\ \eta B_{\perp x} \\ (\Sigma + \kappa T)_x \end{pmatrix}_{\xi}. \qquad \text{(A 1)}$$

https://doi.org/10.1017/S0022377897005941 Published online by Cambridge University Press

$\mathbf{\Sigma}$ denotes $\frac{1}{2}(\mu u^2 + \nu v^2 + \eta {B_\perp}^2)$. For the sake of simplicity, the Hall effect has been neglected and $\mu = \nu = \eta = \kappa$ will be assumed. Inserting $\mathbf{u} = \mathbf{u}((\xi + mt')/\mu = \zeta)$ and integrating once yields the following MHD dynamical system:

$$u_x = m[u] + [p] + \bar{B}_\perp[B_\perp] \equiv \mathbf{\Theta}, \tag{A 2}$$

$$v_x = m[v] - B_x[B_\perp] \equiv \mathbf{\Pi}, \tag{A 3}$$

$$B_{\perp x} = m[\tau B_\perp] - B_x[v] \equiv \mathbf{\Phi}, \tag{A 4}$$

$$\left(\tfrac{1}{2}(u^2 + v^2 + B_\perp^2) + T\right)_x = m[e_t] + [(p + \tfrac{1}{2}B_\perp^2)u - B_x B_\perp v] \equiv \mathbf{\Psi}, \tag{A 5}$$

with $m[\tau] = [u]$ and $\tau p = RT$. In doing this, the following boundary conditions must be satisfied:

$$\lim_{\zeta \to -\infty} \mathbf{u}(\zeta) = \mathbf{u}_L, \quad \lim_{\zeta \to +\infty} \mathbf{u}(\zeta) = \mathbf{u}_R. \tag{A 6}$$

This is a five-dimensional autonomous system of ordinary differential equations for $\mathbf{u} = \mathbf{u}(\tau, u, v, B_\perp, T)$ with a parameter m.

In general, it is very difficult to understand the complicated dynamics of higher-dimensional systems. In MHD, a possible method might be a numerical study using an approximating scheme such as the Runge–Kutta algorithm. For given m and a left state $(\tau, u, v, B_\perp, T)$ at x, numerical integrations of (A 2)–(A 5) will reveal the phase portrait of the MHD dynamical system. However, this method requires tedious calculations, and is inefficient in the sense that we are interested only in profiles connecting singularities. For this reason, we shall adopt the local approach and the global approach based on index theory.

A.2. Singularities

Singularities are determined by $\mathbf{\Theta} = \mathbf{\Pi} = \mathbf{\Phi} = \mathbf{\Psi} = 0$ for given m and a reference state.

When $m = 0$, two singularities (including the reference state) can be found and they represent neighbouring states separated by the contact discontinuity.

When $m \neq 0$, the elimination of $[u]$ and $[v]$ yields the following equations:

$$m^2[\tau] + [p] + \bar{B}_\perp[B_\perp] = 0, \tag{A 7}$$

$$m^2[\tau B_\perp] - B_x^2[B_\perp] = 0, \tag{A 8}$$

with $[\tau] = \tau_L(\mathbf{\Omega} - 1)$. Here $\mathbf{\Psi} = 0$ is incorporated into the density ratio (2.10). These can be rewritten in (U, V) notation as

$$\sigma(\mathbf{\Omega} - 1) + \frac{1}{\gamma}[U] + \bar{V}[V] = 0, \tag{A 9}$$

$$\sigma\{\mathbf{\Omega}[V] + V_L(\mathbf{\Omega} - 1)\} - [V] = 0, \tag{A 10}$$

where $\sigma = \tau_L m^2 / B_x^2$, and $\mathbf{\Omega}$ is given in (2.10). Note that all the singularities can be wholly determined in the reduced (U, V) plane and two running waves represented by $\pm m$ are united in σ.

In conclusion, for given non-zero σ, the MHD vector field can have at most eight singularities, which are projected onto four singularities in the (U, V) plane because (A 9) and (A 10) can be replaced by a quartic polynomial equation. Examples are given in Figs 14(*a–d*). It can be observed that singularities are the intersection of the loop centred at the umbilic point and detached curves similar to a hyperbola.

https://doi.org/10.1017/S0022377897005941 Published online by Cambridge University Press

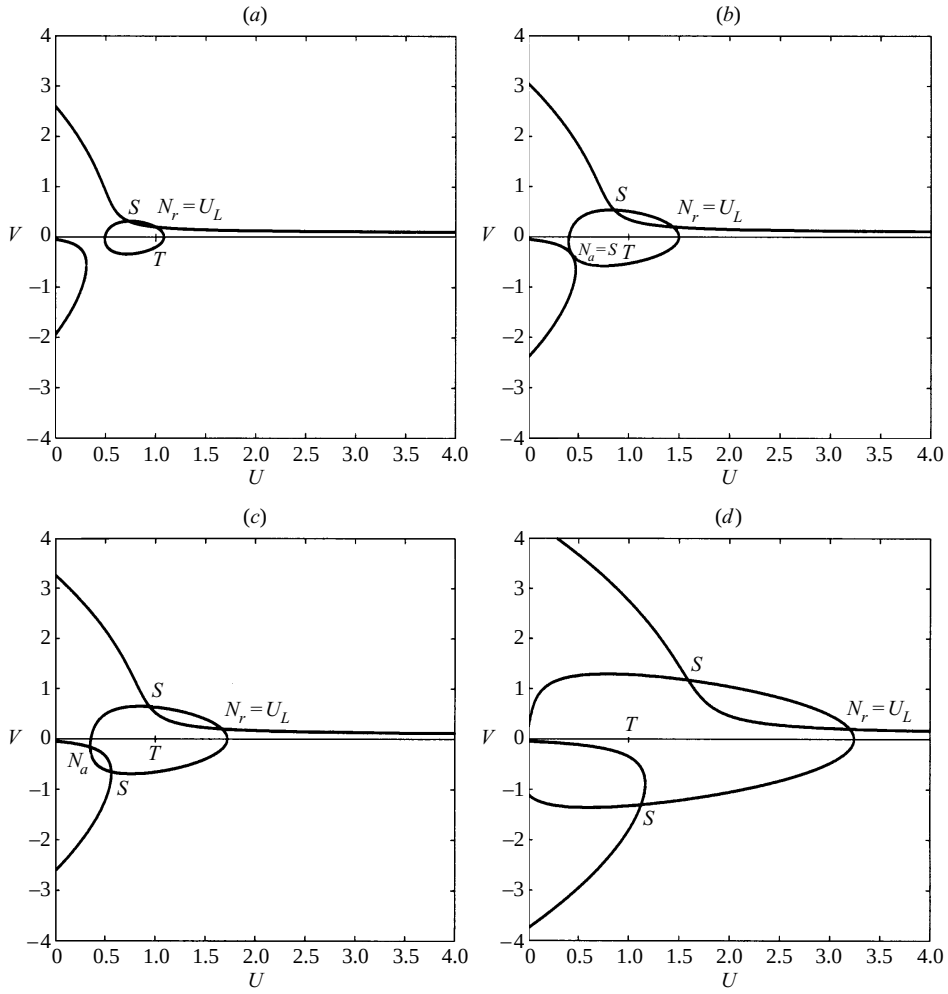


Figure 14. Singularities of MHD shocks: (*a*) $U_L = 1.0$; (*b*) 1.4383; (*c*) 1.667; (*d*) 3.2. $\sigma = 0.64$ and $V_L = 0.2$. N_r, N_a and S denote the repelling node, the attracting node and the saddle respectively.

A.3. Local approach

Singularities in the finite domain can be classified by the sign of the eigenvalues:

$$\frac{c_{f,s}}{\tau} - |m| = \frac{B_x}{\tau_L^{1/2}} \left\{ \mathrm{sign}(B_x) \left(\frac{1 + U + V^2 \pm \{(1 + U + V^2)^2 - 4U\}^{1/2}}{2\Omega} \right)^{1/2} - \sigma^{1/2} \right\}. \tag{A 11}$$

Note that the vector field is symmetrical with respect to the contact discontinuity, and its topology depends only on U and V values of the singularities.

A.4. Global approach

The global approach requires information on the singularities at infinity in addition to the singularities in the finite domain. The singularities at infinity can be obtained by considering the Hugoniot locus, i.e. (2.7), at the umbilic point ($U_L = 1, V_L = 0$).

https://doi.org/10.1017/S0022377897005941 Published online by Cambridge University Press

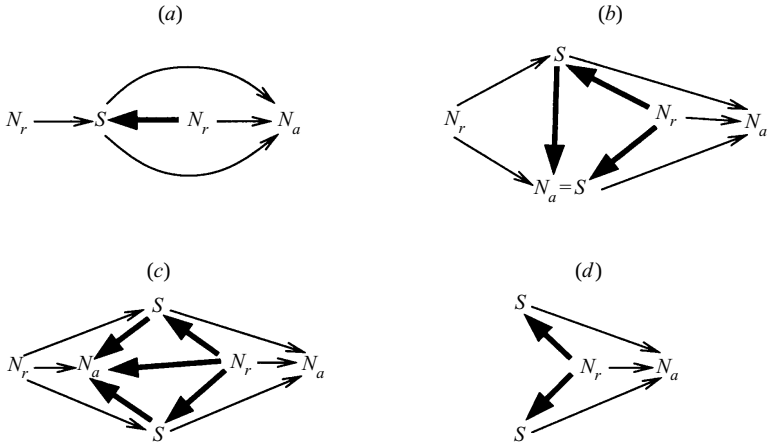


Figure 15. Examples of the global phase portrait for the planar MHD system. Case (*d*) cannot be found in case IV of the 2×2 model system of Part 1 (Myong and Roe 1997*b*). N_r, N_a and S denote the repelling node, attracting node and saddle respectively. The connections from singularities at infinity are indicated by thin solid lines.

In Appendix C, it will be shown that singularities are on the $V = 0$ axis. Hence there are two singularities at infinity, independent of σ. Moreover, they can be classified as nodes, because singularities on $V = 0$ are nothing but singularities in the parallel limit.

On the other hand, it was not determined whether or not the index theory based on the planar system can be applied to only a section of the phase space with higher dimension. Here we presume that it is possible. A justification is that *the MHD dynamical system is invariant under a symmetry transformation*

$$\left.\begin{array}{c} x \leftrightarrow -x, \quad m \leftrightarrow -m, \quad [u] \leftrightarrow -[u], \quad [v] \leftrightarrow -[v], \\ [p] \leftrightarrow [p], \quad [B_\perp] \leftrightarrow [B_\perp], \quad [\tau] \leftrightarrow [\tau]. \end{array}\right\} \tag{A 12}$$

Furthermore, the local analysis also confirms it.

Finally, we demonstrate that the MHD system in the (U, V) plane has at most four singularities in the finite domain, and has two nodes at infinity. The phase portrait of the system consists of two nodes and two saddles in the finite domain. In the case of two singularities, one is a node and the other is a saddle. The configuration with three singularities occurs as a degenerate case or after the attracting-node singularity reaches zero pressure. Examples of the global phase portrait for the MHD system can be seen in Fig. 15. A saddle–saddle connection does not exist, but a node–node connection (which is related to overcompressive shocks) does.

Appendix B. Critical curves

*B.1. The PC*U* curve*

A distinctive feature of Fig. 1 is that Hugoniot curves for some left states have the form of closed loops around the umbilic point, but for other states the loops pass out of the physically meaningful range $U > 0$. Therefore it might be useful to classify the domain by this feature. The domain can be distinguished by the

https://doi.org/10.1017/S0022377897005941 Published online by Cambridge University Press

following critical curve in the (U_L, V_L) plane defined as

$$\left(\frac{\partial U}{\partial V}\right)_{U=0} = 0 \text{ for } V \text{ satisfying (2.7) or (2.9).} \tag{B 1}$$

An example can be found in Fig. 1(*a*). We have from (2.7) that

$$\frac{\gamma-1}{4}\bar{V}[V]^4 - \frac{\gamma-1}{4\gamma}U_L[V]^3 + \frac{U_L}{2}\bar{V}[V]^2 - \left(\frac{U_L}{2} - 1 - \bar{V}^2\right)\frac{U_L}{\gamma}[V] = \frac{\bar{V}}{\gamma^2}U_L^2, \tag{B 2}$$

and, after some manipulation, (B 1) becomes

$$\frac{\gamma-1}{8}[V]^3([V]+8\bar{V}) + \frac{3-2\gamma}{4\gamma}U_L[V]^2 + \frac{\gamma+1}{\gamma}U_L\bar{V}[V] + (1+\bar{V}^2)\frac{U_L}{\gamma} = \frac{\gamma+1}{2\gamma^2}U_L^2. \tag{B 3}$$

We can eliminate V from these equations to give a relation between U_L and V_L. This critical curve is shown by dotted lines in Fig. 4. The origin and U^* given by

$$U^* = \frac{2\gamma}{\gamma+1} \tag{B 4}$$

are located on this curve. Note that parallel slow shocks disappear across U^*. Within the PC^*U^* curve, the Hugoniot curve is a closed loop, and if both states lie within this region then the solution of the Riemann problem is identical to the model. If one state is outside this region then certain waves will not occur. In fact, the remaining classifications have to do with which types of wave are available to create a sign change in V.

B.2. The TC^* curve

In Fig. 1, it can be seen that overcompressive shocks may or may not exist for certain left states. The critical curves for the existence of overcompressive shocks can be calculated in the following way. If $\bar{V} = 0$, (2.32) reduces to

$$[U][V]\{(\gamma-1)[V]^2 + 4(\bar{U}-1)\} = 0. \tag{B 5}$$

For finite V,

$$(\gamma-1)[V]^2 + 4(\bar{U}-1) = 0. \tag{B 6}$$

Using this, the Lagrangian shock speed (2.11) can be written as

$$|m| = \frac{B_x^2}{(\gamma\tau_L)^{1/2}}\{(\gamma+1) - (\gamma-1)V_L^2 - \gamma U_L\}. \tag{B 7}$$

Then the equation $c_{sL}/\tau_L - |m| = 0$ reduces in (U, V) notation to

$$2(\gamma+1)U_L = \gamma|V_L|\{(\gamma-2)^2V_L^2 + 4(\gamma+1)\}^{1/2} - \{(\gamma^2+2\gamma-2)V_L^2 - 2(\gamma+1)\}. \tag{B 8}$$

From Table 1 in Part 1 (Myong and Roe 1997*b*), it can be seen that the overcompressive shock disappears across this critical curve.

The point C^*, which is the intersection of the PC^*U^* and TC^* critical curves, can be calculated by combining (B 1) and (B 6). We have C^* given as

$$\left(\frac{2\gamma(\{2\gamma(\gamma-1)\}^{1/2}-1)}{2\gamma^2-2\gamma-1},\ \pm\left\{\frac{2\gamma+1-\gamma\{2\gamma/(\gamma-1)\}^{1/2}}{2\gamma^2-2\gamma-1}\right\}^{1/2}\right), \tag{B 9}$$

in the (U, V) domain, which is well defined for $1 < \gamma \leqslant 2$ and $\gamma \neq \frac{1}{2}(1+\sqrt{3})$. When $\gamma = \frac{1}{2}(1+\sqrt{3})$, C^* becomes $(\frac{1}{2}(1+\sqrt{3}),\ \pm 12^{0.25}/2)$. The Hugoniot curve at this

https://doi.org/10.1017/S0022377897005941 Published online by Cambridge University Press

special left state is given in Fig. 1(*a*). The curve is tangent to the $U = 0$ axis at C_L ($= B_L = D_L$).

B.3. The C^*U^{**} curve

For some left states, the right states satisfying $c_{sL} - \tau_L|m| = 0$ may be located in the negative-pressure domain. This means that TC^* is no longer critical for the existence of overcompressive shocks. Instead, overcompressive shocks will disappear if the point B_L lies to the left of $U = 0$ (see Figs 1*d*, *e*). Thus we may define the C^*U^{**} curve as

$$c_{sL} - \tau_L|m| = 0, \quad U_R = 0 \quad \text{with the} \quad +R^{1/2} \text{ branch in (2.9).} \tag{B 10}$$

Overcompressive shocks begin to appear across this curve. The curve is calculated numerically. It is easy to show that

$$U^{**} = \frac{2\gamma}{\gamma - 1}, \tag{B 11}$$

by inserting $V_L = V_R = 0$ into $c_{sL} - \tau_L|m| = 0$.

B.4. $C^*\infty$ curve

When the point D_L crosses $U = 0$ (see Figs 1*e*, *f*), slow shocks are no longer available to change the sign of V. The definition is the same as that of the C^*U^{**} curve, except for the branch. Thus it may be defined as

$$c_{sL} - \tau_L|m| = 0, \quad U_R = 0 \quad \text{with the} \quad -R^{1/2} \text{ branch in (2.9).} \tag{B 12}$$

The slow-shock part can be found below the U axis across this critical curve. Note that the point satisfying $c_{sL} - \tau_L|m| = 0$ is a starting point at which the undercompressive shock turns into the slow shock.

B.5. The PU^{**} curve

Fast shocks are no longer available to change the sign of V across this critical curve. The PU^{**} curve can be defined as the Hugoniot passing the origin. Applying this condition to (2.7) yields

$$V_L = \pm\left\{\left(\frac{8U_L}{\gamma(\gamma-1)}\right)^{1/2} - \frac{2U_L}{\gamma}\right\}^{1/2}. \tag{B 13}$$

Appendix C. Proof of $c = \gamma + 1$

The system that we consider is

$$\begin{pmatrix} u \\ v \end{pmatrix}_t + \begin{pmatrix} cu^2 + v^2 \\ 2uv \end{pmatrix}_x = 0. \tag{C 1}$$

As shown by Schaeffer and Shearer (1987), the parameter c controls the behaviour of the system, that is, the wave structure of the system. The properties that distinguish the system by four different cases are the Hugoniot locus of the umbilic point and the $\lambda = 0$ curves. Both properties characterize the general configuration of the Hugoniot. The Hugoniot of the umbilic point can be determined by a cubic equation (Myong and Roe 1997*b*)

$$(2 - c)u^2 v - v^3 = 0. \tag{C 2}$$

https://doi.org/10.1017/S0022377897005941 Published online by Cambridge University Press

And the $\lambda = 0$ curves satisfy the quadratic equation

$$v^2 - cu^2 = 0. \tag{C 3}$$

Then, it can be found that there exist four different cases:

(I) $c < 0$, three Hugoniot lines and a $\lambda = 0$ point;

(II) $0 < c < 1$, three Hugoniot lines and two $\lambda = 0$ lines;

(III) $1 < c < 2$, three Hugoniot lines and two $\lambda = 0$ lines with $(2-c)^{1/2} < c^{1/2}$;

(IV) $2 < c$, a Hugoniot line and two $\lambda = 0$ lines; in some cases, there may exist detached Hugoniot curves.

Then the question is whether there exist similar properties in MHD. From the MHD Hugoniot equation (2.32), the locus of the MHD umbilic point ($U_L = 1,\ V_L = 0$) is determined by

$$V\left(V^4 + \frac{4}{\gamma(\gamma-1)}\left\{1 + (\gamma-1)U\right\}V^2 + \frac{4}{\gamma^2}(U-1)^2\right) = 0, \tag{C 4}$$

with $U \geqslant 0$. Since the term in the large parentheses cannot vanish, there exists only one line, namely, $V = 0$. In addition, from the MHD Hugoniot (2.8) and the model Hugoniot in Sec. 4.1 of Part 1 (Myong and Roe 1997*b*), we can find horizontal asymptotes given as

$$\frac{v_{\max}}{v_L} = \frac{c}{c-2}, \quad \frac{V_{\max}}{V_L} = \frac{\gamma+1}{\gamma-1}. \tag{C 5}$$

Therefore c must be $\gamma + 1$.

On the other hand, the comparison of the $\lambda = 0$ curves with the $c_{f,s} = 0$ curves of MHD is not straightforward owing to $c_{f,s} \neq 0$ for any (U, V). But we can resolve this dilemma by redefining $\lambda = 0$ curves as follows:

$$\bar{v} = 0, \qquad s = \lambda_{sL}, \qquad \text{with} \quad [u] \neq 0. \tag{C 6}$$

It becomes the same as (C 3), since $\bar{u} = s = 0$. By this definition, the $\lambda = 0$ curves represent the boundary that separates the domain by the existence of overcompressive or expansive shocks. Thus in MHD it can be defined as

$$\bar{V} = 0, \qquad \tau_L|m| = c_{sL} \qquad \text{with} \quad [U] \neq 0, \tag{C 7}$$

and is given in (B 8). As shown in Figs 4–6, they consist of two curves passing the umbilic point.

In case of rarefaction waves, we also find that the model and the MHD system are identical in topology, as expected from the fact that the information of rarefaction waves is hidden in the Rankine–Hugoniot conditions.

Finally, we prove that $c = \gamma + 1$.

References

Akhiezer, A. I., Akhiezer, I. A., Polovin, R. V., Sitenko A. G. and Stepanov, K. N. 1975 *Plasma Electrodynamics*, Vol. 1, *Linear Theory*. Pergamon Press, Oxford.

Akhiezer, A. I., Lubarski, G. J. and Polovin, R. V. 1959 The stability of shock waves in magnetohydrodynamics. *Soviet Phys. JETP* **8**, 507–511.

https://doi.org/10.1017/S0022377897005941 Published online by Cambridge University Press

Bazer, J. and Ericson, W. B. 1958 Hydromagnetic shocks. *Astrophys. J.* **129**, 758–785.

Blokhin, A. M. 1994 *Strong Discontinuities in Magnetohydrodynamics.* NOVA, New York.

Brio, M and Rosenau, P. 1994 Evolution and stability of the MHD fast-intermediate shock wave. Preprint.

Brio, M and Wu, C. C. 1988 An upwind differencing scheme for the equations of ideal magnetohydrodynamics. *J. Comp. Phys.* **75**, 400–422.

Ericson, W. B. and Bazer, J. 1960 On certain properties of hydromagnetic shocks. *Phys. Fluids* **3**, 631–640.

Gogosov, V. V. 1961 Resolution of an arbitrary discontinuity in magnetohydrodynamics. *J. Appl. Maths Mech.* **25**, 148–170.

Gomes, M. E. S. 1989 Riemann problem requiring a viscous profile entropy condition. *Adv. Appl. Maths* **10**, 285–323.

Hada, T., Mambu, M., Terasawa, T., Kennel, C. F. and Mjølhus, E. 1993 Evolution of finite amplitude Alfvén waves in space plasmas. *Nonlinear Space Plasma Physics* (ed. R. Z. Sagdeev), pp. 275–283. AIP, New York.

Isaacson, E. and Temple, B. 1988*a* The Riemann problem near a hyperbolic singularity II. *SIAM J. Appl. Maths* **48**, 1287–1301.

Isaacson, E. and Temple, B. 1988*b* The Riemann problem near a hyperbolic singularity III. *SIAM J. Appl. Maths* **48**, 1302–1312.

Isaacson, E., Marchesin, D., Plohr, B. and Temple, B. 1988 The Riemann problem near a hyperbolic singularity: the classification of solutions of quadratic Riemann problems I. *SIAM J. Appl. Maths* **48**, 1009–1031.

Isaacson, E., Marchesin, D. and Plohr, B. 1990 Transitional waves for conservation laws. *SIAM J. Math. Anal.* **21**, 837–866.

Jeffrey, A. and Taniuti, A. 1964 *Non-Linear Wave Propagation.* Academic Press, New York.

Kantrowitz, A. R. and Petschek, H. E. 1966 MHD characteristics and shock waves. *Plasma Physics in Theory and Application* (ed. W. B. Kunkel), pp. 148–206. McGraw-Hill, New York.

Kennel, C. F., Blandford, R. D. and Wu, C. C. 1990 Structure and evolution of small-amplitude intermediate shock waves. *Phys. Fluids* **B2**, 253–269.

Lüst, R. 1955 Stationary magnetohydrodynamic shock waves of arbitrary strength. *Z. Naturforsch.* **10a**, 125–128.

Mann, G. 1995 Simple magnetohydrodynamic waves. *J. Plasma Phys.* **53**, 109–125.

Myong, R. S. 1996 Theoretical and computational investigations of nonlinear waves in magnetohydrodynamics. PhD thesis, University of Michigan, Ann Arbor.

Myong, R. S. and Roe, P. L. 1997*a* Well-posedness of the planar Riemann problem in magnetohydrodynamics. In preparation.

Myong, R. S. and Roe, P. L. 1997*b* Shock waves and rarefaction waves in magnetohydrodynamics. Part 1. A model system. *J. Plasma Phys.* **58**, 485–519.

Naidu, K. and Barnes, A. 1994 Motion of the heliospheric termination shock 4. MHD effects. *J. Geophys. Res.* **99**, 17 673–17 679.

Polovin, R. V. 1961 Contribution to the theory of simple magnetohydrodynamic waves. *Soviet Phys. JETP* **12**, 326–330.

Polovin, R. V. and Demutskii, V. P. 1990 *Fundamentals of Magnetohydrodynamics.* Consultants Bureau, New York.

Roe, P. L. and Balsara, D. S. 1996 Notes on the eigensystem of magnetohydrodynamics. *SIAM J. Appl. Maths* **56**, 57–67.

Schaeffer, D. G. and Shearer, M. 1987 The classification of 2×2 systems of non-strictly hyperbolic conservation laws, with application to oil recovery. *Commun. Pure Appl. Maths* **40**, 141–178.

Shercliff, J. A. 1960 One-dimensional magnetogasdynamics in oblique fields. *J. Fluid Mech.* **9**, 481–505.

Ugai, M. and Shimizu, T. 1994 Computer studies on noncoplanar slow and intermediate shocks associated with the sheared fast reconnection mechanism. *Phys. Plasmas* **1**, 296–307.

https://doi.org/10.1017/S0022377897005941 Published online by Cambridge University Press

Whang, Y. C. 1996 Merging of slow-mode compressive waves in low-β plasma. *J. Geophys. Res.* **101**, 2529–2534.

Wu, C. C. 1987 On MHD intermediate shocks. *Geophys. Res. Lett.* **14**, 668–671.

Wu, C. C. 1988*a* The MHD intermediate shock interaction with an intermediate wave: Are intermediate shocks physical? *J. Geophys. Res.* **93**, 987–999.

Wu, C. C. 1988*b* Effects of dissipation on rotational discontinuities. *J. Geophys. Res.* **93**, 3969–3982.

Wu, C. C. 1990 Formation, structure, and stability of MHD intermediate shocks. *J. Geophys. Res.* **95**, 8149–8175.

Wu, C. C. 1995 Magnetohydrodynamic Riemann problem and the structure of the magnetic reconnection layer. *J. Geophys. Res.* **100**, 5579–5598.

https://doi.org/10.1017/S0022377897005941 Published online by Cambridge University Press